An Experimental Characterization of the Steady State Behavior of a Spur Gear Pair

UNDERGRADUATE HONORS THESIS

Presented in Partial Fulfillment of the Requirements for Graduation with Honor's Research Distinction in the Department of Mechanical Engineering at The Ohio State University

By

Brian Anichowski, Jr

Undergraduate Program in Mechanical Engineering

The Ohio State University

2016

Thesis Committee:

Dr. Ahmet Kahraman

Dr. Jason Dreyer

Abstract

Dynamic Transmission Error (DTE), or the difference between the ideal and actual positions of the output gear in a gear pair, is a common metric utilized to evaluate the dynamic characteristics of a spur gear pair. Studies most commonly investigate gear pair noise and vibrations, yet the underlying mechanisms leading to noise and vibrations are not fully understood. Variations introduced by the manufacturing processes such as tooth indexing errors complicate the gear pair dynamics further. However, prior to understanding the impacts these variations have on gear pair dynamics, a no-error baseline data set must be created as a means of experimental comparison.

In order to completely characterize the dynamic behavior of the gear pair, and therefore develop this no-error database, a setup that can operate a gear pair under tightly-controlled dynamic conditions is required as well as dedicated accelerometer based DTE measurement system. This research developed such a measurement system to acquire high-frequency vibration data, as well as a digital data processing scheme to compute DTE. With the focus on characterization of the baseline behavior with no tangible manufacturing errors, a set of experiments was performed within a wide range of operating speeds (sweep up from 500 to 4200 rpm and sweep down from 4200 to 500 rpm) and torque loads (100-300 Nm). The results were then examined in the frequency domain to develop a complete characterization of the no-error spur gear pair through the creation of waterfall plots and

root-mean-square forced response curves. These plots were then used to establish the baseline resonance behavior depending upon system operating conditions. In addition, further analysis was completed to highlight the apparent softening type nonlinear behavior due to intermitted loss of contact and natural frequency increase seen with increased transmitted torque load.

Dedication

To my family and friends.

Acknowledgements

I would like to thank Dr. Kahraman, my advisor, for his support and guidance throughout this work. I would also like to thank Sam Shon for his substantial help during experimental testing, along with David Talbot for his seemingly endless depth of knowledge and Jonny Harianto for his support and encouragement. Thank you to all of my colleagues for their willingness to help with any task, no matter the size. In addition, thank you to the Gear and Power Transmission Laboratory Consortium members for their continued support and for ultimately allowing me to pursue and complete this work, and for Dr. Jason Dreyer for serving on my defense committee.

Finally, thank you to my friends, for their endless support and motivation, and to my family, to whom this would not have been possible without.

Vita

1993.....Born in Columbus, Ohio

May 2012.....Olentangy Liberty High School

Powell, Ohio

August 2015 to Present…….....Research Associate, GearLab

Fields of Study

Major Field: Mechanical Engineering

Table of Contents

List of Tables

List of Figures

Chapter 1:

Introduction

1.1 Background and Motivation

One main functional requirement of gear systems is that they must be quiet. If not appropriately designed for, vibrational amplitudes originating from gear meshes might often be large enough to cause the gearbox housing and surrounding structures to vibrate, introducing gear noise as well as higher dynamic stresses into the gear pair. In automotive transmission design, mitigating the impact of these vibrations is imperative, as customers demand quiet and reliable vehicles. As with any noise and vibration problem, the most effective solution to the gear noise in automotive transmissions is to control it at its source; the gear mesh. For this, it is essential to understand the mechanisms leading to gear vibration excitations at the gear meshes, and to design gear pairs which are able to control such excitations. Equally critical is the impact of various manufacturing errors within allowable tolerance limits, as these deviations from the intended design impact the same noise generation mechanisms.

As elaborated in detail in Ref. [1], motion transmission error of the gear pair is a widely accepted parameter correlating the vibratory behavior of the gear pair to the

resulting noise. It is defined in Ref. [1] in a purely torsional sense as "the difference between the actual position of the output gear and the position it would occupy if the gear drive were perfectly conjugate." Transmission error (TE) is defined mathematically along the line of action of the gear pair as

$$TE(t) = r_p \hat{\theta}_p(t) + r_g \hat{\theta}_g(t), \tag{1.1}$$

where r_p and r_g are the base circle radii of the pinion *p* (driving gear) and gear *g* (driven gear), respectively. Here $\hat{\theta}_p(t)$ and $\hat{\theta}_g(t)$ are the instantaneous positions of the pinion and gear defined in terms of nominal kinematic rotations and deviations (vibrations) from these nominal rotations as $\hat{\theta}_p(t) = \omega_p t + \theta_p(t)$ and $\hat{\theta}_g(t) = -\omega_g t + \theta_g(t)$. Given the gear ratio relationship of $r_p \omega_p = r_g \omega_g$, Eq. (1.1) can be reduced to $TE(t) = r_p \theta_p(t) + r_g \theta_g(t)$. This indicates that the instantaneous deviations of rotational motions from the nominal ones define the transmission error.

With the assumption that transmission error can be considered as a metric for how the amount of vibrations the gear pair will produce, various design practices were developed to minimize it. Under loaded conditions, gear teeth in mesh deflect to form an elastic component to TE. This deflection can be neutralized by intentionally removing material from the involute tooth surface profile. If such tooth modifications (tooth "corrections" in the form of negative material) are equal in magnitude to that of the elastic deformations, TE is eliminated at that "design" load, in the process achieving a quiet gear pair. In addition, TE can help quantify the impact unintentional manufacturing errors of the

gear teeth have on the gear pair and the resulting geometric deviations from the designed profile, which can then be addressed through manufacturing process optimization. For this, the gear designer must have knowledge of the impact profile errors have on transmission error, and hence, the required quality level of the gear pair for the given noise requirements.

This undergraduate research study aims to provide a foundation for an accompanying graduate study focusing on the impact a class of manufacturing errors have on the dynamic behavior of a gear pair in the form of TE. The baseline behavior defined by the elastic deformations and the designed tooth modifications cannot be separated in a product application from the behavior induced by manufacturing errors, posing the question of whether the poor tooth modifications are the reason for noise or the manufacturing errors. Through controlled lab experiment, this study will establish the baseline dynamic behavior of a gear pair have no errors such that the sole contributions of manufacturing errors to gear vibrations can be quantified in the future. By developing this baseline database, along with the accompanying data acquisition system, further experimental testing can be completed as a means to quantify the vibrational dynamics induced by manufacturing errors.

As a means of clarification, different variations of TE must be defined up front. As it is done in most gear load distribution models, TE is often predicted under quasi-static conditions (gear rotating at very low speeds with little or no dynamic effects) and is known as Static Transmission Error (STE). Optical encoders connected to the gears rotating at a very low speed can be used to measure STE under both loaded (Loaded Static Transmission Error (LSTE)) and unloaded (Unloaded Static Transmission Error (USTE)) conditions. Likewise, accelerometer based measurement systems can be used to measure TE under

actual operating speed conditions where dynamic effects are prominent. This type of TE, called Dynamic Transmission Error (DTE), is the main concern of this study.

1.2 Literature Review

1.2.1 Dynamic Transmission Error Measurement System

Transmission Error as a metric of gear vibration was originally developed by Harris as a means to understand the vibrational amplitudes seen in gear sets [2]. His work was instrumental in the development of transmission error as a concept, and set the framework for future studies. Initial measurement methods were rudimentary at best, particularly at high speeds, due to the simplicity of sensors and limitations of the analog data acquisition devices. However, shortly after Harris' development of transmission error, Tordion and Gerardin [3] developed a robust measurement system involving two tangentially mounted accelerometers in order to negate the effects of gravity. This system, albeit applied in a more modern fashion herein, is the underlying methodology used for this study.

Despite the viability of the initial accelerometer based system, significant work developing various other experimental methods was completed over the following decades. Most of these methods were explained within a literature review on the topic completed by Munro [4]. His review details the limitations with the most conventional industrial method, single flank testing, at speed, and briefly discusses viable alternatives.

Munro's survey of transmission error measurement methodology served as a decent review of the work immediately following Harris' initial development. However,

substantial improvements were made to test methodology over the following twenty-five years. Smith [5] highlighted many of these improvements in his book, and provided a detailed explanation of the benefits digital signal acquisition and processing has versus the conventional analog system. In addition, Blankenship and Houser [6] experimentally studied many of the common transmission error measurement systems, and provided a significant amount data outlining the strengths and weaknesses of each system. In particular, their study highlighted the substantial benefits of accelerometers at high speed, which is the application used within this study.

As Smith [5] explained, many of the drawbacks surrounding an accelerometer based transmission error measurement system shown in Munro's work were negated with the advent of digital signal acquisition. The various digital metrics greatly increased the practicality and feasibility of accelerometer based measurement techniques. This led to many studies utilizing accelerometer based measurement systems, such as those completed by Heskamp [7] and Kang and Kahraman [8], both at Ohio State. Both of these studies utilized an accelerometer array to dynamically capture vibrational data, and then used a quasi-integration technique to quantify the transmission error of the gear set. These configurations allowed for a much higher frequency (>10kHz) data capture than conventional analog methods, and the use of accelerometers can be attributed to the very high accuracy measurements within these studies, which would have been otherwise unattainable with typical encoder style measurement systems.

1.2.2 Basic Spur Gear Dynamics

Due to significant industry interest, a substantial amount of research has been completed in the area of basic spur gear dynamics, and therefore a wide breadth of knowledge exists in the area. More specifically, an exhaustive catalog of studies has been developed explaining the baseline conditions surrounding standard operation of no-error parallel axis spur gears, with most research particularly focusing on the vibrational excitations seen across large ranges of operating conditions.

Most of these studies, in some form, built upon the equations and models of spur gear pairs developed – in conjunction with experimental databases – by Gregory et al [9, 10]. They worked extensively to develop a suitable set experimental studies explaining the "dynamics of heavily loaded, high-speed spur gears with very small manufacturing errors", which very similarly follows the intent of a portion of the research here.

Their initial experimental work was instrumental in the development of the spring-mass gear pair model introduced by Tuplin in 1953 [11]. They applied many of the dynamic effects seen in their initial experimental testing into a substantial refinement of Tuplin's model, helping to develop one of the first time-variant stiffness models [9]. This model was further refined by Cornell and Westervelt almost twenty-five years later [12], to roughly resemble the current model upon which most modern gear research utilizes. These models can be used to accurately and reliable predict the experimental dynamics seen in minimal error spur gear pairs. For instance, Velex [13] utilized these models as a starting point for his three-dimensional spur gear models which far exceeds the complexity of both the work of Gregory at al [9, 10], as well as this accompanying thesis.

These models [9-12] were experimentally validated and theoretically refined over the course of the next thirty years, with significant focus being given to dynamic factors and stress (as these represented most industry concerns). Lin and Liou's work [14] focused on a full dynamic stress and load analysis of a spur gear pair, while Seiger and Houser [15] experimentally validated a dynamic loading model for spur gears, amongst many others. These studies, while focused primarily on dynamic factors and loading characteristics, simultaneously investigated many of the underlying vibrational dynamics. As such, many investigations into the dynamic causes of gear mesh excitations and the related dynamic loads were also completed during the validation of these dynamic loading models, with a significant depth of material on the topic being included within Ozguven and Houser's extensive literature review [16].

1.2.3 Non-Linear Behavior of Spur Gears

While most of these initial studies provided a solid understanding of the fundamental dynamics seen within minimal-error spur gear pairs, more recent research has been focused upon extending these studies in order to characterize the extensive nonlinear behavior seen in even the most basic of spur gear pairs. Furthermore, specific interest has been taken to understand the nonlinear behavior directly around the primary resonance frequency. For instance, Kahraman and Singh [17] built upon existing dynamic models in order to further model the significant jump nonlinearities seen about the primary mesh frequency. The nonlinear solutions presented therein were then compared to previous

experimental results to provide a mathematical explanation for the then unknown phenomena.

Kahraman and Singh's work led to such studies as Kahraman and Blankenship [18-20], all of which investigated specific dynamic nonlinearities seen within minimal-error spur gear pairs. Work by Kubur et al. [21], which applied the same conditions to helical gear pairs, showed that such nonlinear behavior is not evident in helical gears. Studies such as Litek et al. [22] built upon Cornell and Westervelt's [12] work to include these nonlinearities into complex mathematical models, most of which investigated topics far outside simple gear dynamics. These studies all developed substantial theoretical and experimental data sets upon which this thesis hopes to both experimentally validate (at least in part) and build upon.

1.3 Objectives and Scope

The main objectives of this thesis are listed as follows:

(i) develop an accurate and repeatable measurement system designed to capture the vibrational dynamics seen in the gear pair,

(ii) build an efficient data analysis system to determine the DTE seen in both transient and steady state conditions, and

(iii) develop a full characterization of the dynamic behavior of a minimal-error spur gear pair.

The scope of this work will be kept limited to the dynamic behavior of gears having no tangible manufacturing errors. The methodology and results of this study are intended to form the baseline for a MS thesis on the influences of manufacturing errors on DTE.

1.4 Outline

Chapter 2 introduces the experimental test setup and procedures. It provides the working principles of a back-to-back high-speed gear dynamics test machine first, followed by details of the accelerometer based DTE measurement system, along with an explanation of the data acquisition and digital data analysis systems. Test procedures to allow operation under both steady-state and transient conditions are also outlined. Chapter 3 provides a complete set of data collected under both of these conditions. These measurements are discussed in terms of the resonance activity, nonlinear behavior and dependence on the torque transmitted. Finally, Chapter 4 summarizes this study and lists a number of conclusions as well as lessons learned and provides a prelude to the Master's thesis to follow.

Chapter 2:

Test Methodology

2.1 Introduction

This chapter will discuss the data acquisition and analysis procedures used in this study, starting first with an explanation of the test machine used as well as the gear specifications for the minimal-error spur gear pair. An accelerometer based measurement system, similar to that used in both Heskamp [7] and Kang and Kahraman [8], will then be described, with emphasis on deviations from their work. This discussion of the measurement system used will include an explanation on the accompanying LabVIEW and MATLAB programs created for both steady-state and transient data collection and analysis.

2.2 Machine Setup

An earlier version of the test machine utilized within this study was previously developed by Kahraman and Blankenship [18-21, 23, 24] as a means to measure and

quantify many of the non-linear dynamic behavior seen in spur gears. For this purpose, the machine was designed with the intent to minimize vibrational interactions between the test gear pair and other rotating components of the machine, especially the reaction gearbox. Figure 2.1(a-b) shows the machine used in this study. While a full discussion of the machine design is not warranted here, as a thorough explanation is included within the above references [18-21, 23, 24], some specific design features will be explained due to their direct relevance to this study.

Since this test intended to capture the vibrational dynamics of a test gear pair, vibrational isolation of the test gear pair from the surrounding environment was imperative. Primary means of vibration isolation of the test pair primarily focused on shaft and bearing design. Each shaft is supported in four locations, one on either side of both the reaction and test gear pairs, with large, well lubricated bearings. By reducing the lengths of unsupported shaft between bearing locations, shaft deflections are minimized during operation. In addition to these considerations, the test machine also utilizes long, torsionally compliant shafts with elastomer couplings to reduce potential reaction gear pair and shaft disturbances from interacting with the vibrational dynamics captured at the test pair. These details can be more readily seen in Figure 2.1(b), with a top down schematic of the test machine also shown as Figure 2.2. In addition to these machine design considerations, specific focus was given to the design of the actual gear sets used. Both the reaction and test gear sets are unity ratio pairs, signifying a 1:1 ratio between tooth counts for each gear within each set. In addition, as will be explained later, the test gear pairs and reaction gear pairs have non-interacting tooth counts, being 50:50 and 63:63, respectively. The specific tooth counts utilized are significant as they produce different mesh orders across the useable frequency

(a)

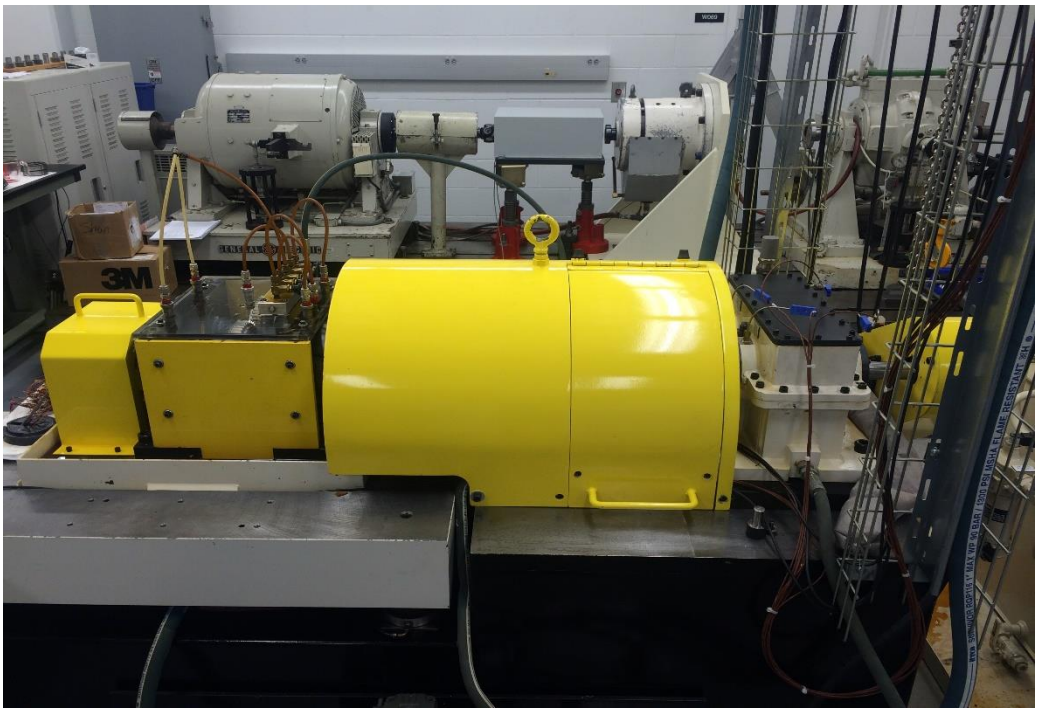

(b)

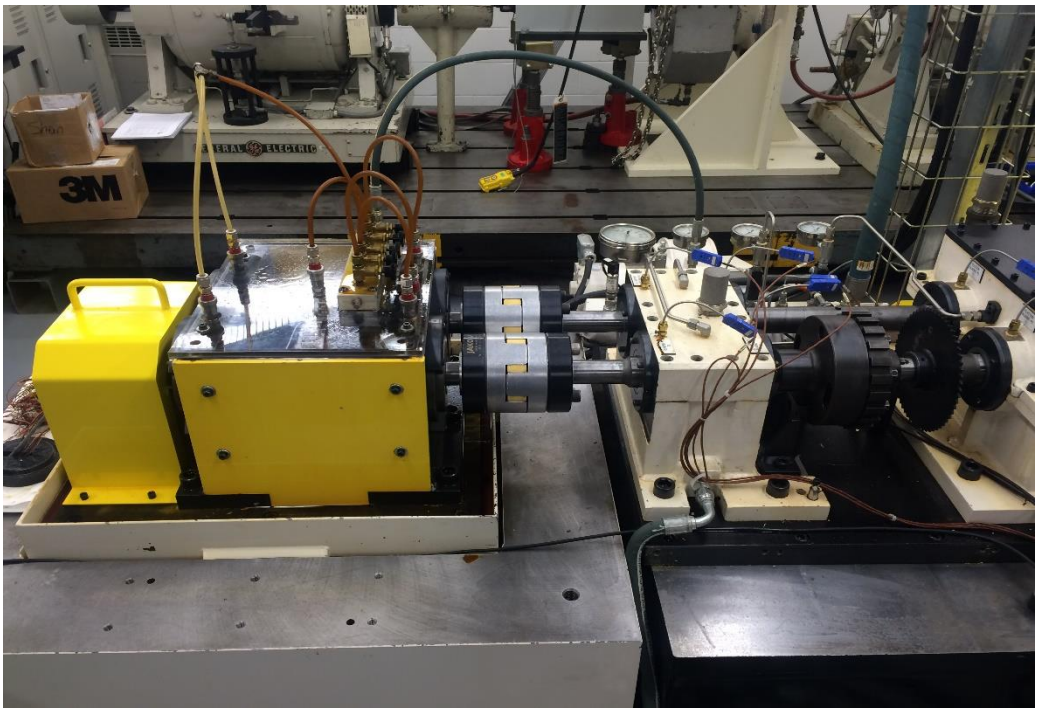

Figure 2.1: Picture showing test machine with (a) safety covers on and (b) safety covers removed.

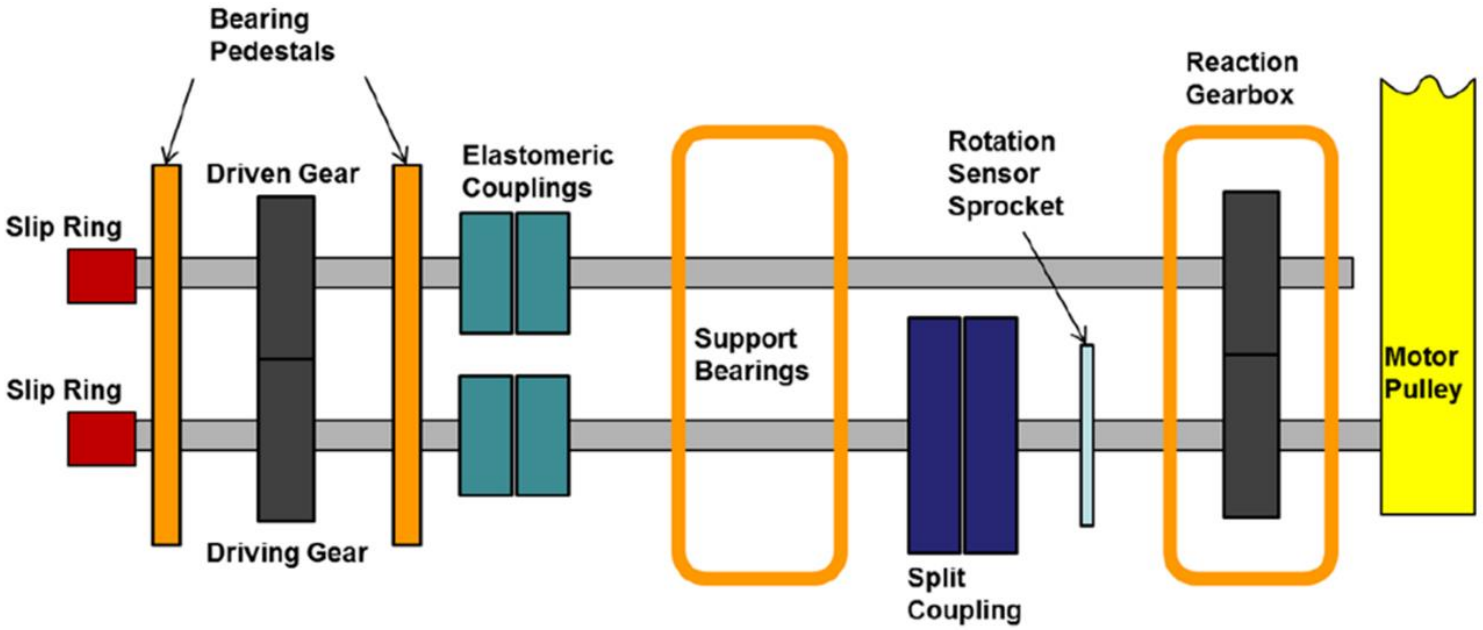

Figure 2.2: Top view schematic of dynamic test machine (adapted from Ref. [25]).

range of the accelerometers, allowing for easy identification, and filtering and removal (if needed) during data analysis.

Beyond the need to isolate the reaction gear pair and the test gear pair, the machine was also designed using a “four-square” closed loop in order to allow for mechanical loading of the gear pairs. This loading is completed as shown in Figure 2.3, through the use of a locking pin applied to one flange of a split coupling while a moment arm with calibrated weights applied torque to the other flange of the coupling. This “four-square” closed loop, often referred to as a “back-to-back” configuration, is crucial in ensuring the constant-torque loaded gear mesh conditions required for a full spur gear pair characterization are met. As well, this closed loop allows for a seemingly undersized motor to drive the gear pair at high loads and speeds with no issue, with the system maximum speed nearing 7000 rpm introducing dynamic effects well outside the usable frequency range of most commercially available accelerometers.

In addition to these vibration isolating design features, the machine was also purpose-built for the particular accelerometer based measurement system used here, as explained at length in many previous studies [7, 8, 18-21, 23, 24]. Of particular note are the flange supports located along the face of each gear, as well as the locking mechanism used to fix the torsional and axial position of each gear to its associated shaft. Firstly, by providing a flange support upon which the accelerometers are mounted, and directly pinning the gear through this support, any torsional misalignments between the test gear and accelerometer(s) are mitigated. Secondly, by using a locking lag-nut to ensure no axial motion of the test gear pair, any relative motion between each gear, and between the gear pair and the test machine, is removed. These two design considerations greatly improve the

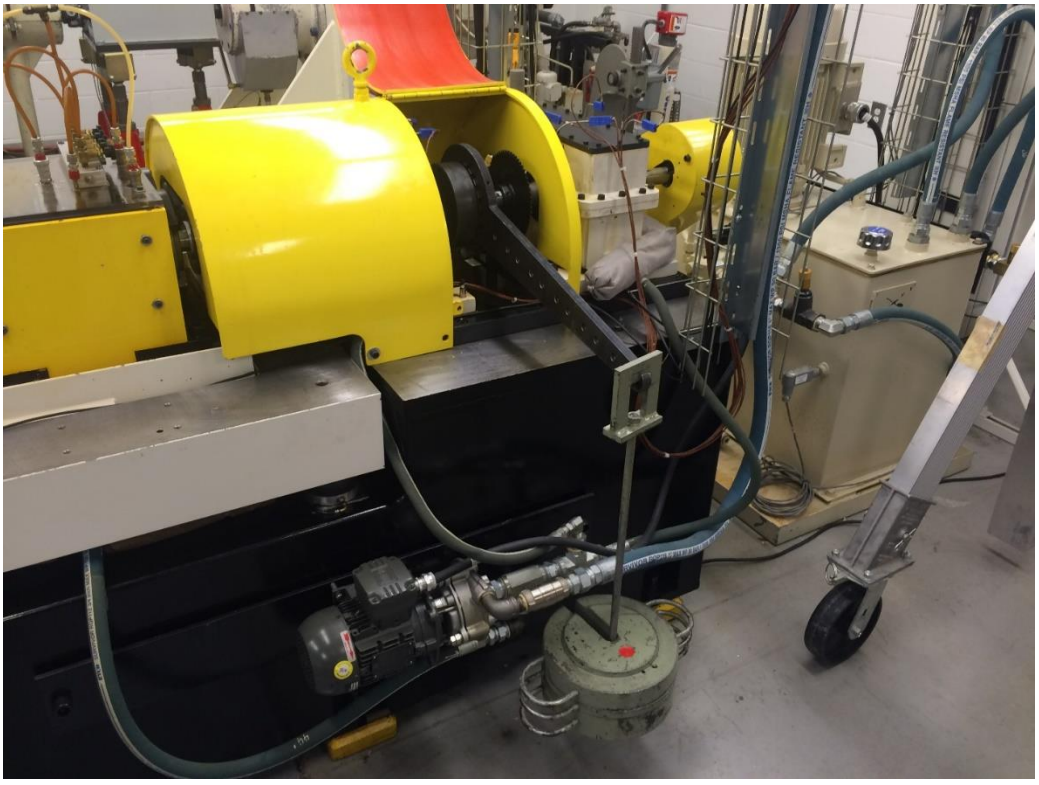

Figure 2.3: Mechanical loading of dynamic test machine to the four-square closed loop using moment arm at split coupling.

viability of high-speed and high-accuracy dynamic testing.

The test machine is controlled by an Allen Bradley PLC, which manages the speed of a small DC motor connected to the dynamics machine input shaft via a pulley drive, along with real-time monitoring of the machine's lubrication and coolant systems. This setup allows complete control of the system speed, including steady state testing as well as transient testing with specified ramp speeds (in rpm/s) and dwell times. Through the use of this speed control system, along with the closed-loop mechanical loading configuration previously explained, testing can be completed in both sweep up and sweep down configurations from between two speeds at any user defined torque value.

2.3 Gear Specifications/Matrix

The minimal error gear pair utilized in this study was used extensively in previous studies, including Kahraman and Blankenship [19, 23, 24] as described previously. More recently, Sun [25] utilized this gear pair to investigate the impact of tooth indexing errors on tooth root stresses. His work explained the exact gear specifications used at length. Of particular note for this study are the inclusion of tip-relief cuts as a means to mitigate transmission error, as shown in Kahraman and Blankenship [20], Munro [26], and Palmer [27]. As well, the test gear pair was designed with a 1.75 contact ratio, signifying that for 75% of the mesh cycle, two tooth pairs are loaded, while the remaining 25% of the mesh cycle only has one tooth loaded. Basic parameters of the test gear pair are listed in Table 2.1 [25].

Table 2.1: Basic Spur Gear Parameters (from Ref. [25])

Parameter [unit]	**Value**
Number of Teeth	50
Normal Module [mm]	3.00
Pressure Angle [deg]	20.0
Pitch Diameter [mm]	150.0
Base Diameter [mm]	140.95
Major Diameter [mm]	156.00
Minor Diameter [mm]	140.68
Circular Tooth Thickness [mm]	4.64
Active Fact Width [mm]	20.0
Tip Relief Magnitude [mm]	0.01
Starting Roll Angle of Tip Relief [deg]	20.9

As this study aims to develop a minimal-error baseline condition to be used in subsequent studies, two high-precision ground gears with minimal indexing errors were employed. In order to verify the condition of these gears prior to use, a detailed metrological study of the pair was completed [25]. Figure 2.4 shows profile and lead traces for the primary no error gear, labelled as “Gear #1” from this point forward. The accompanying no error gear, “Gear #2”, showed similar levels of profile deviation, and can therefore also be classified as a minimal-error gear. A picture of the two gears used can be seen in Figure 2.5.

2.4 Measurement/DAQ Setup

The accelerometer-based measurement system is adapted from Heskamp [7] and Kang and Kahraman [8], and relies heavily upon the work done therein. Any deviations of their methodology will be described in length in subsequent sections. With that being said, most of the specific information located within the following two subsections will heavily build upon the work of these two.

2.4.1 Dynamic Transmission Error Measurement System

As previously mentioned, this study utilized an accelerometer based dynamic transmission error measurement system. This measurement system is comprised of tangentially mounted uniaxial accelerometers at a radial mounting distance, ρ, from the axis of rotation of a gear. This radial mounting position is similar in radial length to the

(a)

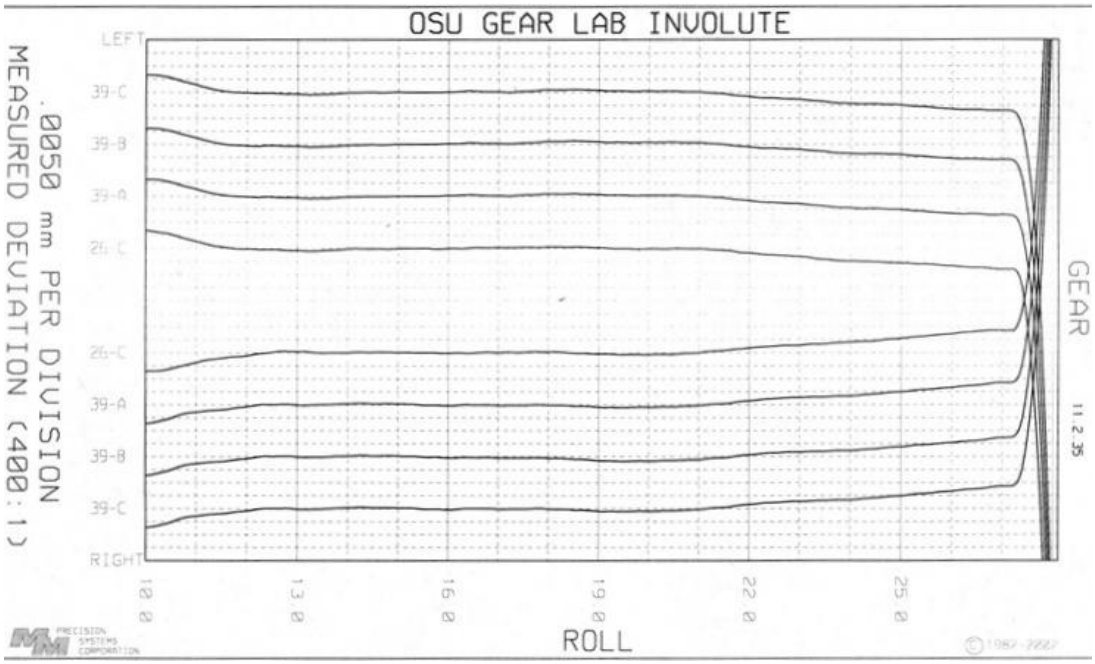

(b)

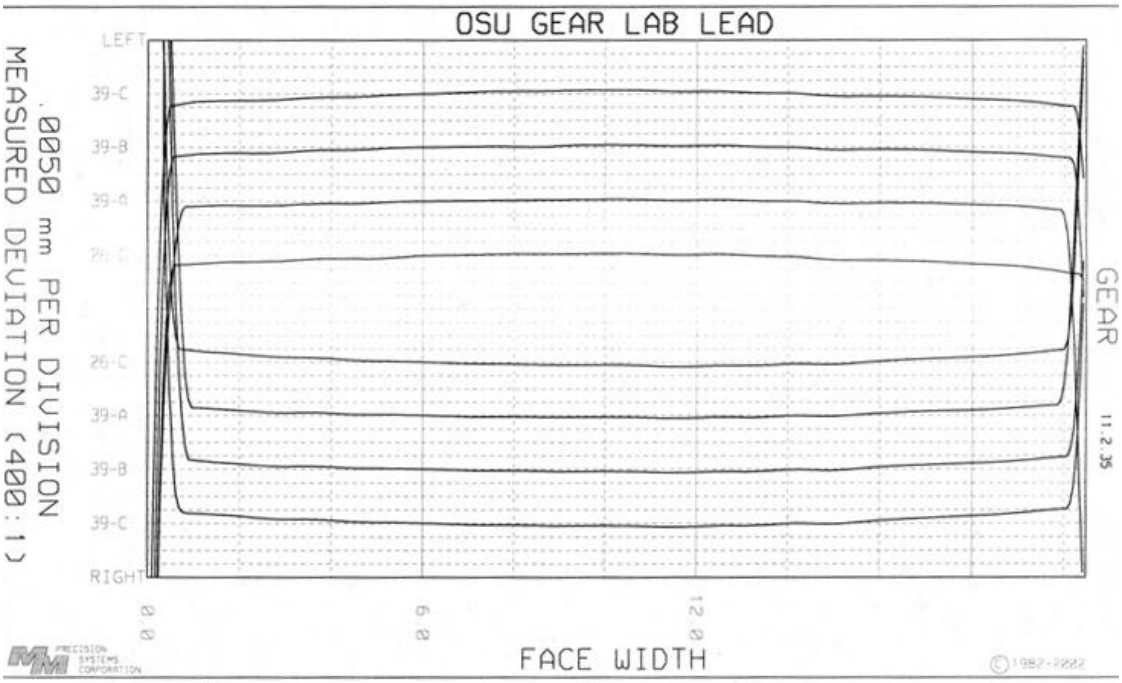

Figure 2.4: (a) Profile and (b) Lead traces of minimal error spur gear #1 (from Ref. [25])

Figure 2.5: No-error spur gear pair used in this study.

base radius of the gear pair, typically given as r_i, where $(i = p, g)$. While the test setup described in Section 2.2, has the capabilities to use four accelerometers mounted at 90 degree increments on each gear, only two will be required for this study, as described in Heskamp's work [7].

These accelerometers, due to their diametrically opposing mounting setup, capture acceleration signals that can be added to negate the effects of gravity. A picture of the accelerometer setup on is shown in Figure 2.6(a), with a schematic of the setup shown in Figure 2.6(b). The individual accelerometer signals $a_{1T}(t)$ and $a_{2T}(t)$ capture the tangential (circumferential) acceleration of the instrumented gear as

$$a_{1T}(t) = \rho\ddot{\theta}_g(t) + g\sin(\omega_g t), \tag{2.1a}$$

$$a_{2T}(t) = \rho\ddot{\theta}_g(t) - g\sin(\omega_g t) \tag{2.1b}$$

where $\ddot{\theta}_g(t)$ is the angular acceleration to be captured for the instrumented gear, ω_g is the angular velocity of the gear, and g is the gravitational acceleration. By summating $a_{1T}(t)$ and $a_{2T}(t)$ in these two equations, any gravitational effects are cancelled and a generalized rotational acceleration of the individual gear can be attained as

$$\ddot{\theta}_g(t) = \frac{1}{2\rho}\left[a_{1T}(t) + a_{2T}(t)\right]. \tag{2.2}$$

The same methodology can be applied to determine the angular acceleration of the other gear (pinion), $\ddot{\theta}_g(t)$, as well.

(a)

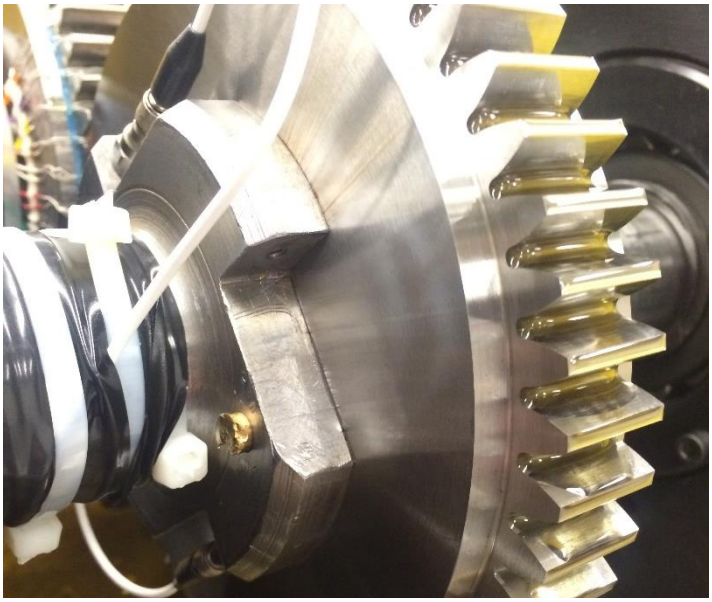

(b)

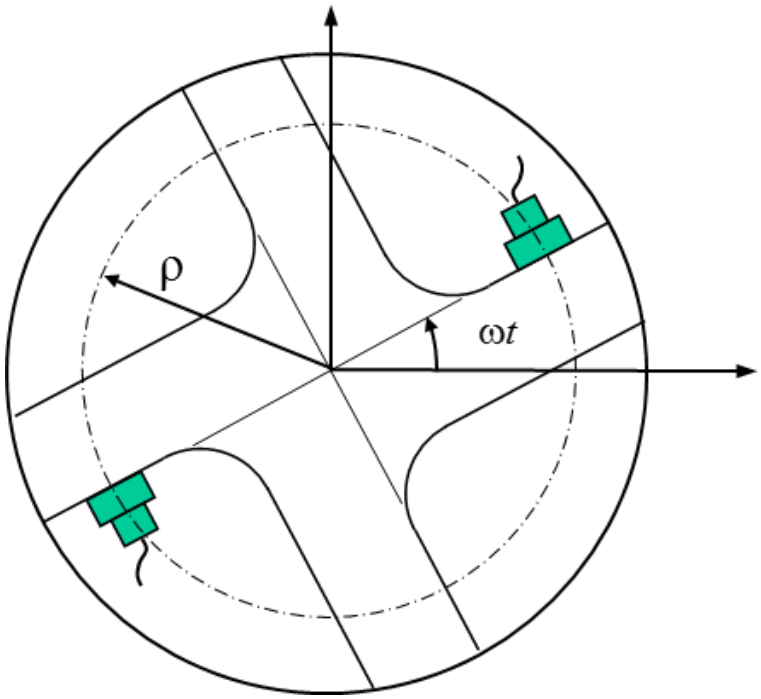

Figure 2.6: (a) Diametrically opposed accelerometers mounted onto a flange on the face of the gear, with (b) an accompanying schematic adapted from Ref. [8].

The typical method to calculate the resultant DTE from this point, as has been done in previous studies [7, 8], is to instrument both gears with an identical measurement system. This allows the measurement system to capture the individual acceleration of each gear, and the resultant DTE can be found by integrating twice and adding both signals together, as

$$DTE(t) = \iint \left[r_p \ddot{\theta}_p(t) + r_g \ddot{\theta}_g(t) \right] dtdt , \tag{2.3}$$

which is shown graphically with a block diagram in Figure 2.7.

However, this study takes advantage of the symmetric nature of the unity gear pair, as previously explained, to reduce the complexity of this equation and accompanying measurement system. Due to the nature of the dynamic models previously described [9-12], the symmetry of the gear pair ensures that all deviation from perfectly conjugate motion is seen equally in both gears. This can be utilized to simplify the data acquisition greatly, as the system only requires one set of accelerometers to entirely capture the motion of the gear pair. The resultant DTE from one gear can be multiplied by two in order to capture the DTE of the pair, given as

$$DTE(t) = 2\iint \frac{r}{2\rho} \left[a_{1T}(t) + a_{2T}(t) \right] dtdt , \tag{2.4}$$

where $r = r_p = r_g$ for these test gears.

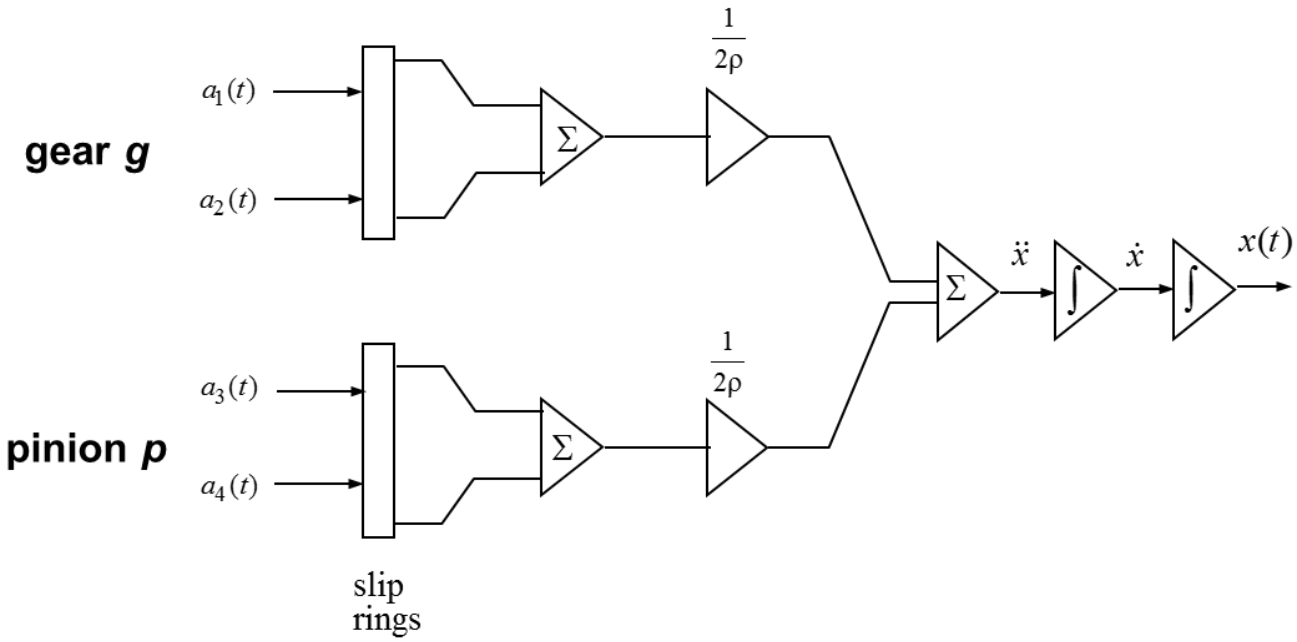

Figure 2.7: Block diagram showing the calculation for dynamic transmission error.

2.5 DAQ Set-up

Data acquisition for this study closely follows the setup developed by Kang and Kahraman [8], and utilizes much of the same equipment. A schematic of the data acquisition system can be seen in Figure 2.8.

This study utilized two uniaxial accelerometers (PCB Piezotronics 353B18) with a useable frequency up to 10 kHz. These accelerometers were primarily chosen for their reasonably large frequency range, which allowed for little loss of data beyond the primary mesh frequency of the system. In particular, at the fastest proposed test speed, the accelerometers selected captured the first three mesh harmonics with little to no signal loss, while the fourth and fifth harmonics provided useable frequency data. The gear and accelerometer mounting considerations previously explained, coupled with the large useable frequency range of the accelerometers, allowed for accurate and reliable data collection across all operating conditions of interest.

The signal from each accelerometer was initially passed through the hollow shafts upon which the gears are mounted, and connected to a 10 channel slip ring (Michigan Scientific SR10M) located on the end of the shaft. This can be seen in Figure 2.9. These signals were then combined into a coaxial connection (one cable for each accelerometer), and sent through a multichannel signal conditioner (PCB Piezotronics ICP 483M92) for ICP based sensor excitation and basic signal amplification. The signals were then sent through an analog-to-digital converter (National Instruments PXI-4472) which was loaded into a general purpose data acquisition chassis (National Instruments PXI-1042). All data acquisition was controlled through LabVIEW programs, being purpose built for either

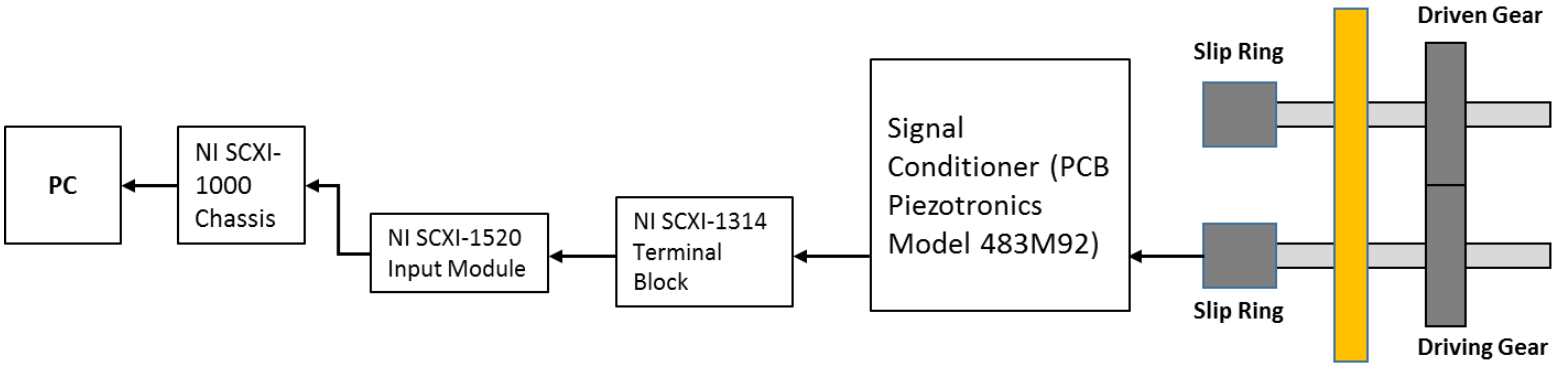

Figure 2.8: Block diagram and schematic of the data acquisition system used in this study.

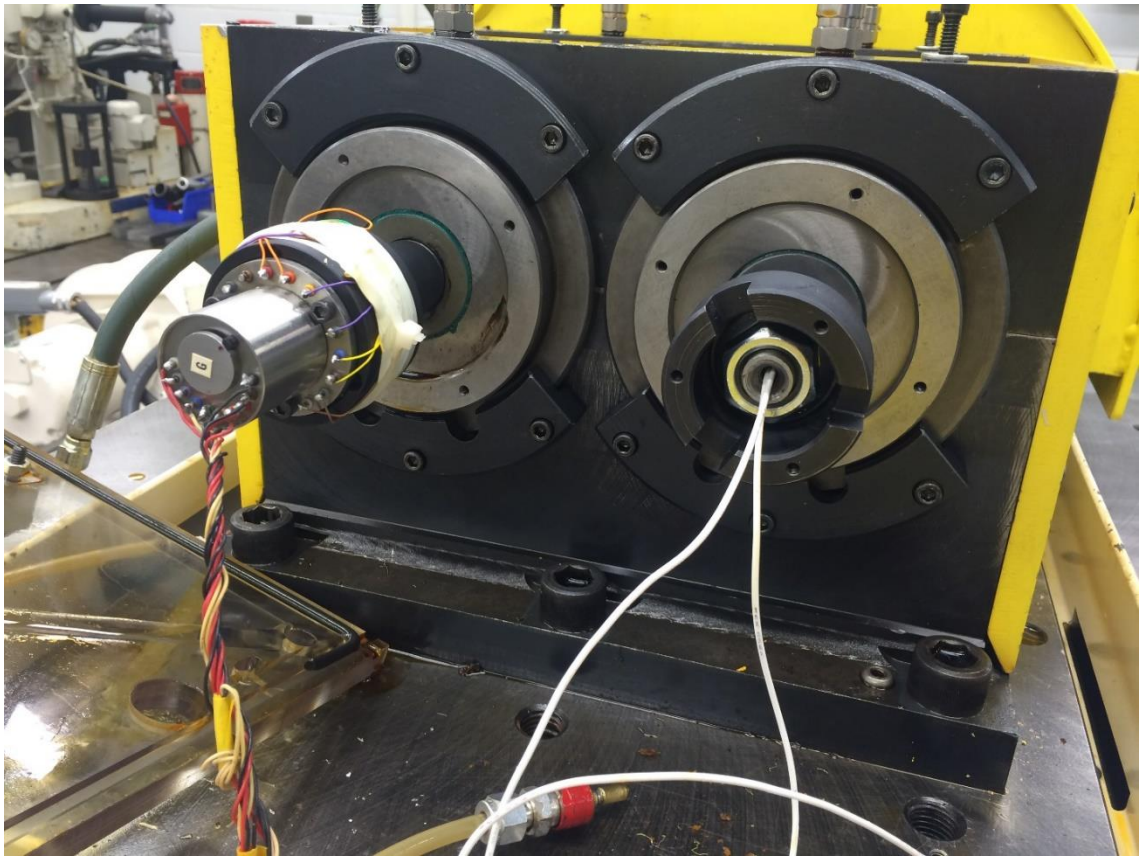

Figure 2.9: The right shaft shows the hollow configuration through which the wires from the accelerometer(s) were passed, while the left shaft shows an example of the 10-channel slip ring utilized in this study.

steady state or transient data collection. Figure 2.10(a-b) shows the physical data acquisition system used for this study.

2.6 LabVIEW Set-up

Two separate LabVIEW programs were developed for this study. Each LabVIEW program was tasked with simply collecting data, as opposed to the programs developed by both Heskamp [7] and Kang and Kahraman [8], which were also tasked with machine speed control and data collection. This is due to the inclusion of the machine speed controller, as previously explained in Section 2.2.

The first LabVIEW program was developed for the steady-state testing, and was designed in order to verify steady-state condition at each intermittent speed (50 rpm increments used in this study with the range of 500 rpm to 4200 rpm). In order to do this, the LabVIEW program monitored the motor speed using a 60-tooth-per-rev tachometer, and referenced this value against the previous second of data. If ten seconds of continuous motor speed was attained (±1.5 rpm), the LabVIEW program collected one second of acceleration data at a sampling frequency of 100 kHz. This sampling rate was well above the 20 kHz Nyquist frequency of the accelerometers.

The second LabVIEW program was developed for the transient testing. This data collection did not require any complicated verification systems as the operating conditions were intended to be dynamic in nature. However, some issues arose due to the limitations of the computer used during data acquisition, along with the significant increase in the amount of data per data set, and therefore testing frequency was reduced to 40 kHz. Despite this reduction, the testing frequency was still two times the Nyquist frequency, ensuring

(a)

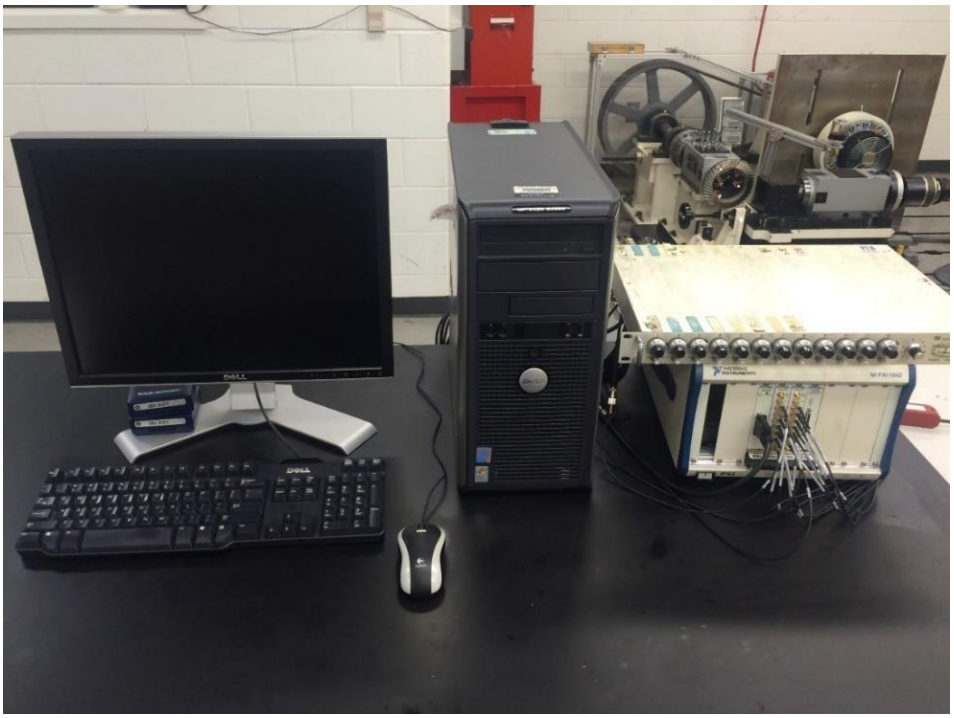

(b)

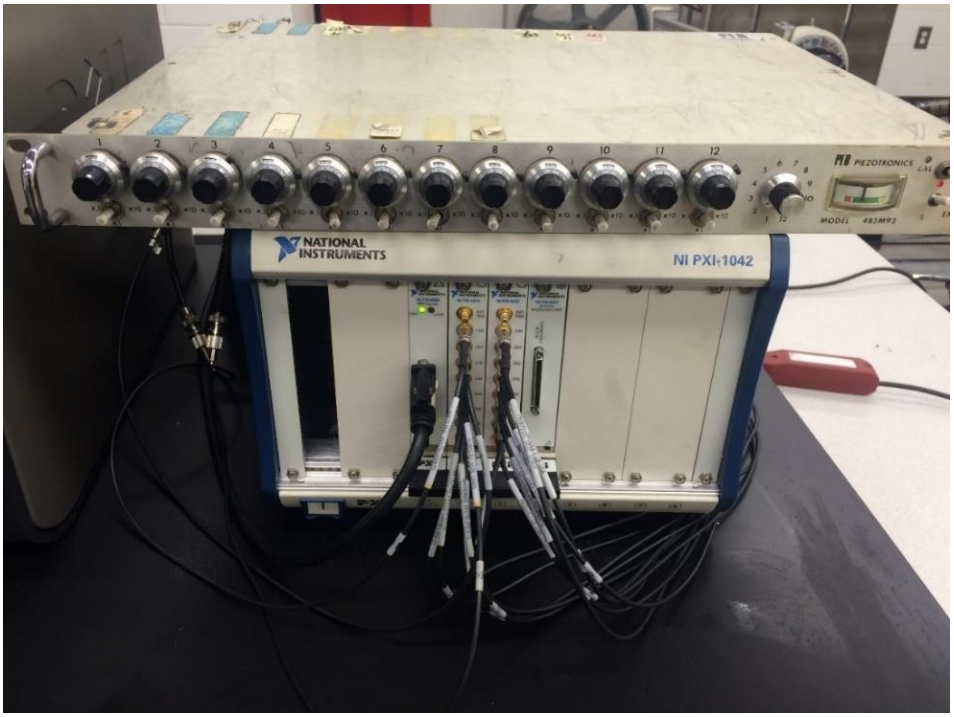

Figure 2.10: (a) The measurement system utilized for this study and the (b) signal conditioning and data acquisition hardware.

accurate data collection. Transient data collection occurred over a six-and-a-half-minute sweep, with a three-minute sweep up (500 rpm to 4200 rpm), a thirty second dwell at the maximum speed (4200 rpm), and a three-minute sweep down (4200 rpm to 500 rpm) in order to compile a large enough data set for analysis.

2.7 MATLAB Set-up

2.7.1 Steady State Tests

A steady-state program was developed in accordance with the mathematical procedure explained in Section 2.4.1, starting with loading in the raw acceleration signals captured from each steady state speed increment. Each data set was scaled and combined in order to provide the general acceleration of the gear, following Eq. (2.2). The Fast Fourier Transform (FFT) was then taken of each data set to convert from the time domain to the frequency domain. Double integration of this frequency domain signal was then completed using pseudo-integration techniques, following the logic that

$$\iint A\sin(\omega t)dtdt = -\frac{A}{\omega^2}\sin(\omega t)\,. \tag{2.5}$$

This pseudo-integration provided the magnitude of position deviation at each point along the computed frequency spectrum, following Eq. (2.3). The resultant DTE of each speed increment was then found as a root-mean-square (RMS) sum of the first five mesh harmonics of DTE, in the form

$$DTE_{rms} = \sqrt{\sum_{n=1}^{5} A_n^2}\,, \tag{2.6}$$

where A_n represents the magnitude of the n^{th} mesh harmonic order at frequency nf_{mesh} ($f_{mesh} = \frac{1}{2\pi} N_g \omega_g$ where N_g is the number of teeth of gear *g*). This procedure was repeated for each discrete speed value at various constant torque levels for both sweep up and sweep down conditions.

2.7.2 Transient Tests

The transient data set was processed in much the same way as the steady-state data set. However, as noted previously, transient data was collected in one large, single data file. In order to accurately compute the DTE across the transient sweep, the large data set (encompassing a several minute long sweep) was broken into quasi-steady state data sets (each set being 0.3875 seconds) and processed in the steady state manner described above. These quasi-steady state data sets were then recompiled to create a full transient data set across the entire operating range. A point of note is that the sweep up and sweep down sections within the larger data set were kept separate, and the dwell data was discarded as it served little purpose for the goals of this study.

Chapter 3:

Experimental Results

3.1 Introduction

This chapter presents and discusses the experimental results from the tests performed according to the test matrix and procedures described in Chapter 2. Section 3.2 will present the DTE measured across the ranges of speed and torque for both steady-state and transient operation. Section 3.3 and 3.4 will discuss the observed dynamic effects of the gear pair in order to develop a full characterization of the minimal-error baseline condition. As a whole, this section will focus on the linear and basic nonlinear dynamics of interest, with the understanding that a more in-depth analysis is not explicitly required for the purposes herein.

3.2 Dynamic Transmission Error Measurements

All dynamic transmission error (DTE) data presented within this section were collected for the minimal-error gear pair with the gear parameters previously defined in

Table 2.1. Measurements were taken from 100 Nm to 300 Nm in 100 Nm increments, and from 500 rpm to 4200 rpm, in both sweep up and sweep down considerations. As well, transient and steady-state data was collected as a means of further characterization of the spur gear pair.

3.2.1 Steady-State Measurements

Plots containing the calculated FFT signal of the minimal-error spur gear pair at selected speeds of interest for the steady-state condition are shown in Figure 3.1 at 300 Nm. These plots show the frequency spectra of DTE that was calculated using Eq. (2.4) at $\Omega = 800$, 950, 1300, 1850 and 3700 rpm, corresponding to gear mesh frequencies of $f_{mesh} = \frac{1}{60} N\Omega = 667$, 792, 1083, 1542 and 3083 Hz where $N = 50$ teeth. The differences between the 100Nm, 200Nm, and 300Nm test conditions will be further explained in Section 3.4. Several observations can be made from these frequency spectra. Firstly, besides the low frequency content below 250 Hz, all of the spectra are dictated by a family of harmonic orders that are interrelated. The first five (and the only significant ones) of these frequencies are marked along the *x* axes by red "x" symbols. It is evident that these harmonic components represent the fundamental mesh frequency (f_{mesh}) and its higher harmonics ($2f_{mesh}$, $3f_{mesh}$, $4f_{mesh}$ and $5f_{mesh}$) representing the 2nd to 5th harmonic of DTE. It also indicates that the measurement and data acquisition systems devised are capable of collecting clean (noise free) signals consisting solely of DTE harmonics.

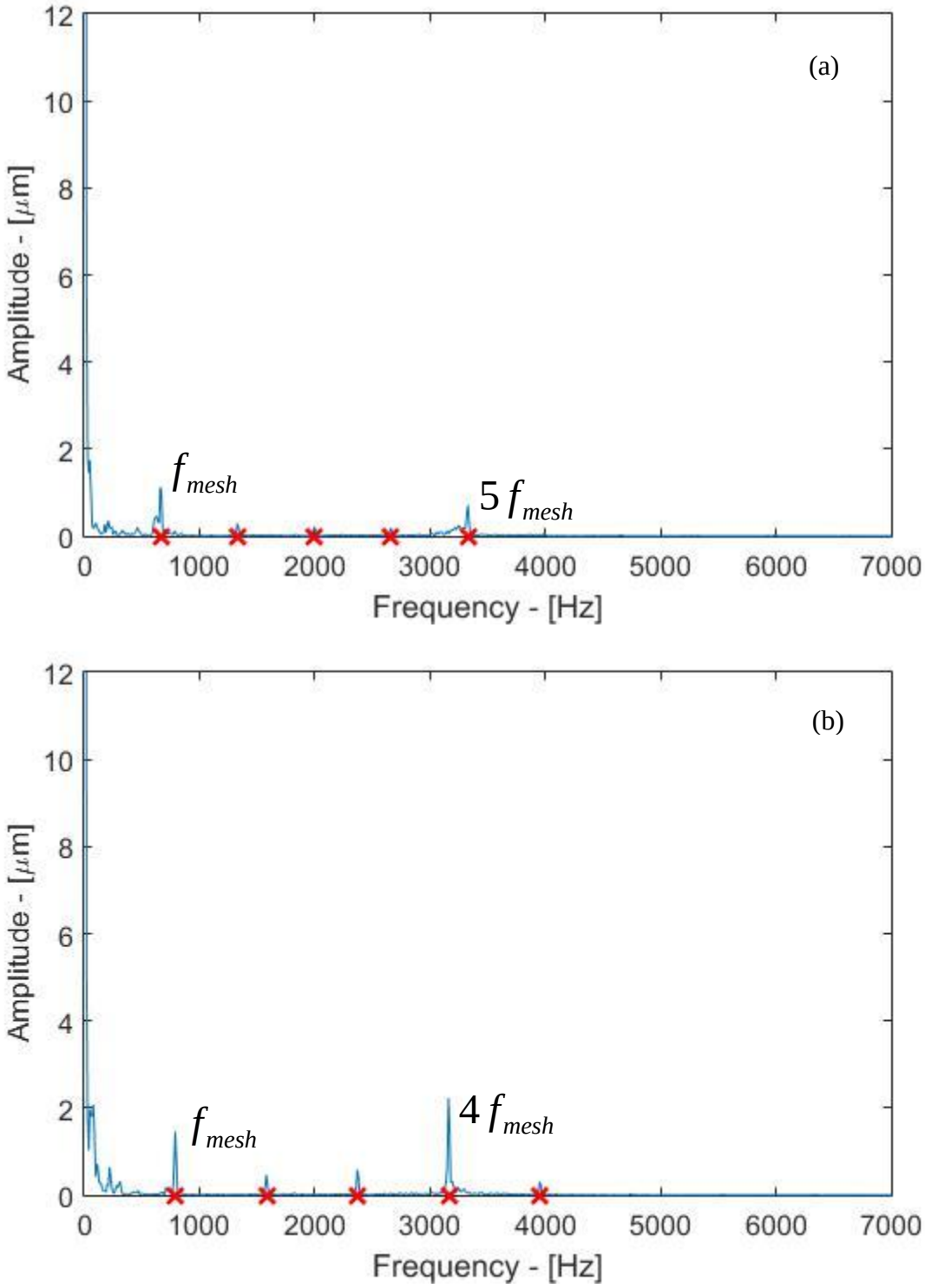

Figure 3.1: Scaled FFT Signal of Dynamic Transmission Error at each super-harmonic resonance for (a) 800 rpm (b) 950 rpm (c) 1300 rpm (d) 1850 rpm and at the primary resonance of (e) 3700 rpm for 300Nm transmitted torque load during sweep up testing.

Figure 3.1 continued.

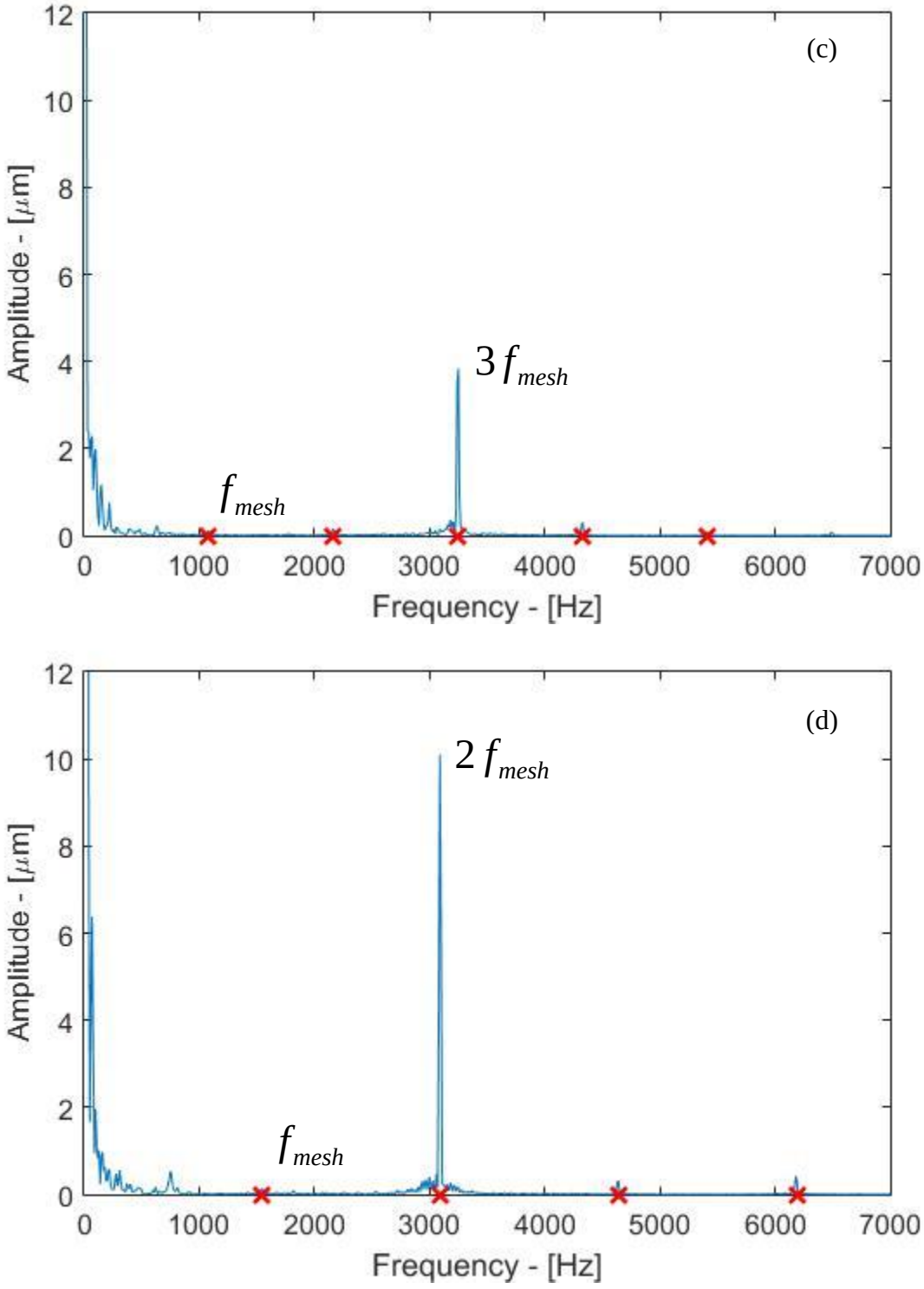

Figure 3.1 continued.

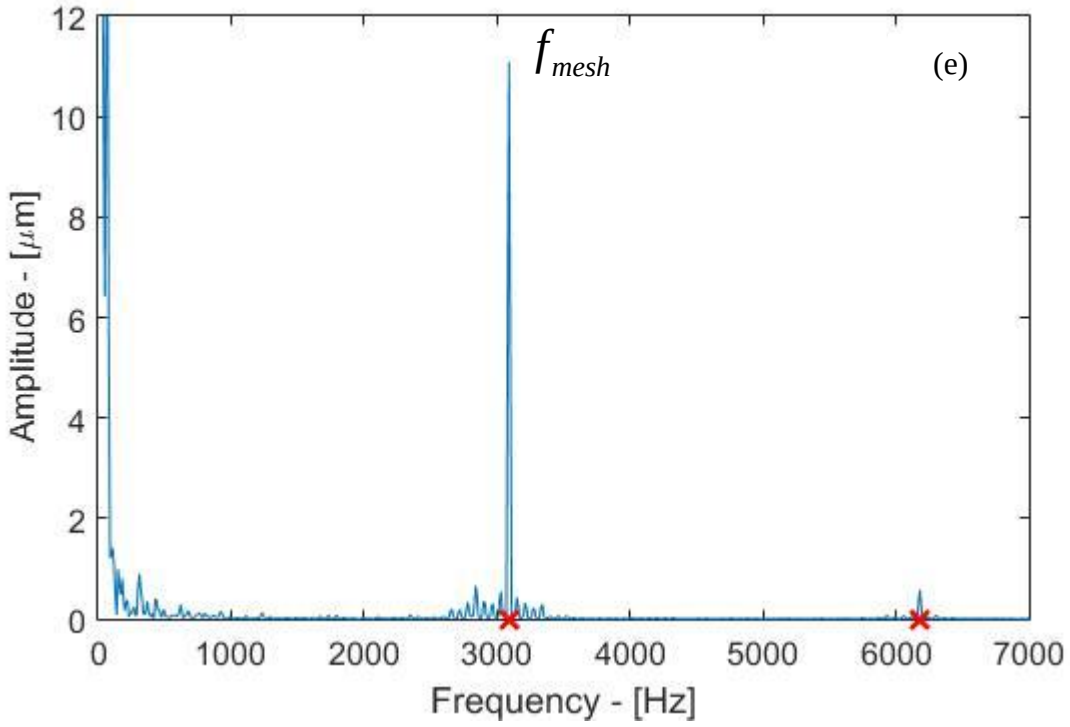

In Figure 3.1(a) at $\Omega = 800$ rpm, ($f_{mesh} = 667$ Hz), the highest amplitude harmonic order is the 5th harmonic $5 f_{mesh} = 3,335$ Hz. In Figure 3.1(b) for $\Omega = 800$ ($f_{mesh} = 792$ Hz), the 4th harmonic at $4 f_{mesh} = 3,168$ Hz has the largest amplitude. Likewise, the 3rd, 2nd, and fundamental harmonic amplitudes are the largest in Figure 3.1 (c), (d) and (e) at $3 f_{mesh} = 3,249$ Hz, $2 f_{mesh} = 3,084$ Hz, and $f_{mesh} = 3,083$ Hz, respectively. This collectively indicates the torsional natural frequency f_n of the gear pair is within the range of 3,000-3,300 Hz, as each of the spectra in Figure 3.1 represent a resonance condition of $f_n = i f_{mesh}$ ($i \in [1,5]$). This natural frequency for a purely torsional gear pair (having very rigid bearing supports and shafts, as it is the case here) behaving linearly is defined as [16, 17, 23, 24]

$$f_n = \frac{1}{2\pi}\sqrt{\frac{\bar{k}_{mesh}}{m_{eq}}}\,, \tag{3.1}$$

where $\bar{k}_{mesh}$ is the average value of the gear mesh stiffness and m_{eq} is the equivalent gear pair mass that is defined in terms of polar mass moments of inertia, I_p and I_g, and base radii, r_p and r_g, of the mating pinon and gear as

$$m_{eq} = \frac{I_p I_g}{I_p r_g^2 + I_g r_p^2}\,. \tag{3.2}$$

The above equations represent a reduced dynamic model having constant and linear stiffness. In the case of a spur gear pair, as studied here, the mesh stiffness fluctuates as the number of tooth pairs in contact changes with rotation of the gears. As such,

$k_{mesh}(t) = \bar{k}_{mesh} + \tilde{k}_{mesh}(t)$, not simply $k_{mesh}(t) = \bar{k}_{mesh}$ [18-19]. Furthermore, the same spring is subject to a clearance due to backlash, causing tooth separations and a softening type nonlinear behavior. These aspects of the dynamics of the spur gear pairs tested in this study will be illustrated in several points in the rest of this chapter.

With the DTE frequency spectrum at each steady-state speed increment established, as illustrated in Figure 3.1, steady-state forced response curves that plot room-mean-square (RMS) DTE amplitudes against f_{mesh} are presented next in Figure 3.2(a-c) at 100, 200, and 300 Nm, respectively. Here, the RMS amplitudes of DTE are calculated from the amplitudes of the first five mesh harmonics using Eq. (2.6). These forced response curves closely match those measured by Hotait and Kahraman [28] using the same gear set considered in this study.

In Figure 3.2(a-c), two sets of data points are plotted; one set as the speed is increased (sweep up) in a steady-state incremental method, and another set as the speed is reduced in the same incremental manner (sweep down). These sets agree with each other in the ranges where the spur gear system is linear (i.e. where no tooth separation occurs), while they differ in the apparent resonance ranges due to nonlinear behavior. It is evident in Figure 3.2 that there is a fundamental resonance within the range of 2500-3300 Hz, representing the resonance condition of $f_{mesh} = f_n$. In addition, super-harmonic resonance peaks are present at $f_{mesh} = \frac{1}{2} f_n$ (or $f_n = 2 f_{mesh}$) and $f_{mesh} = \frac{1}{3} f_n$. It is also clear that these resonance frequencies increase (shift to the right) with an increase in torque transmitted, which will be discussed later.

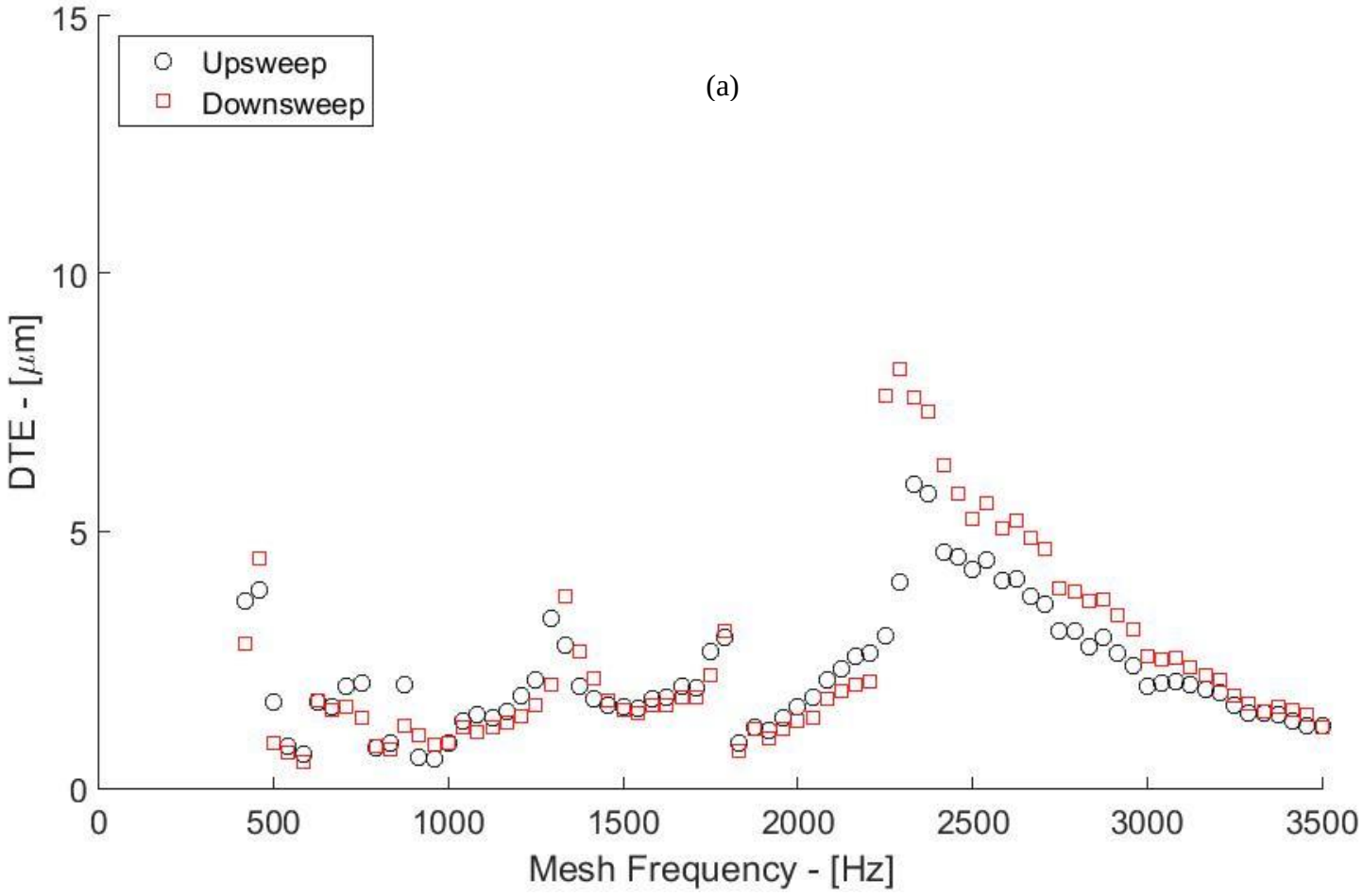

Figure 3.2: RMS Dynamics Transmission Error measurement for (a) 100Nm, (b) 200Nm, and (c) 300Nm of transmitted torque for sweep up and sweep down operation.

Figure 3.2 continued.

(b)

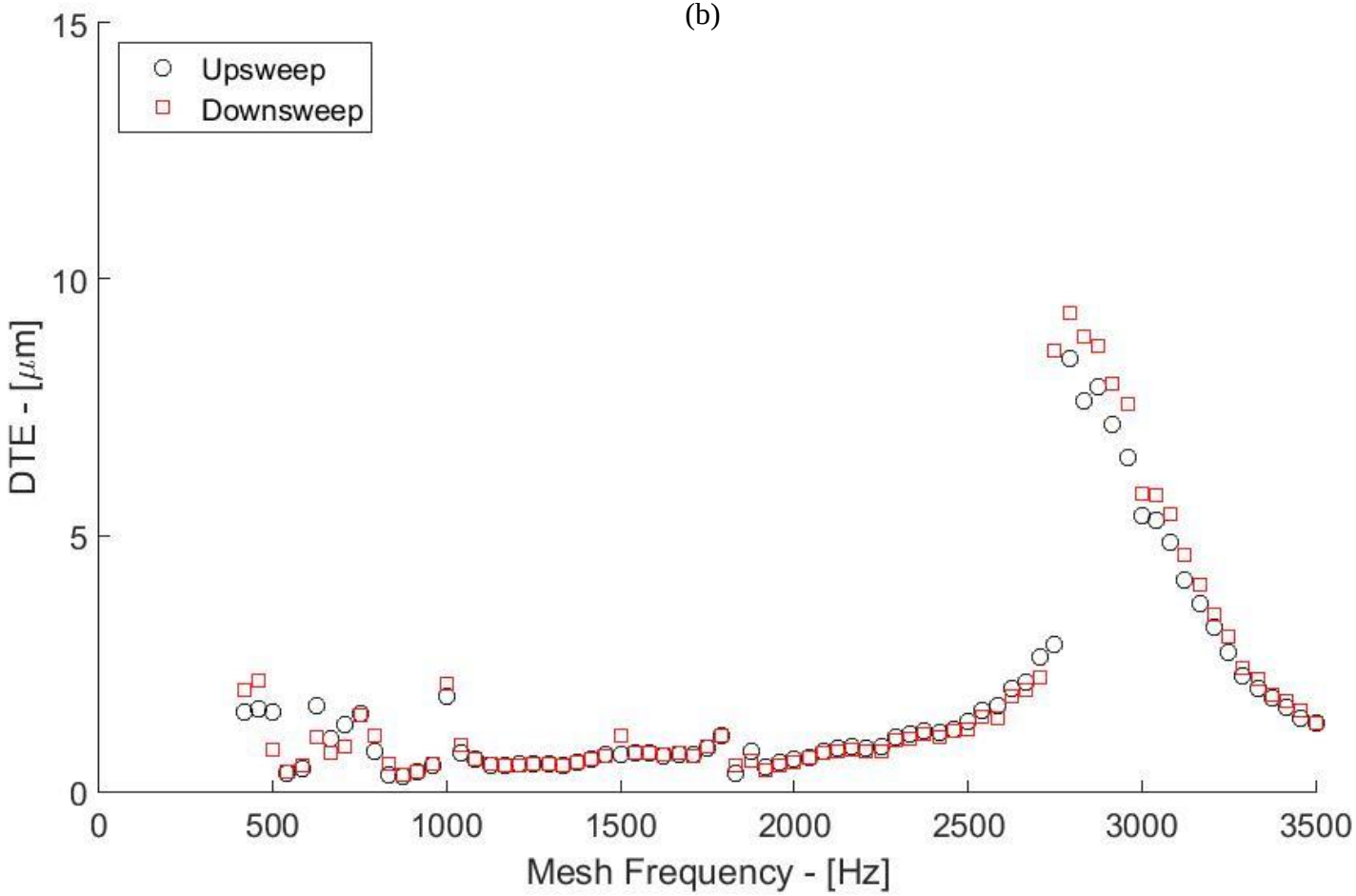

Figure 3.2 continued.

(c)

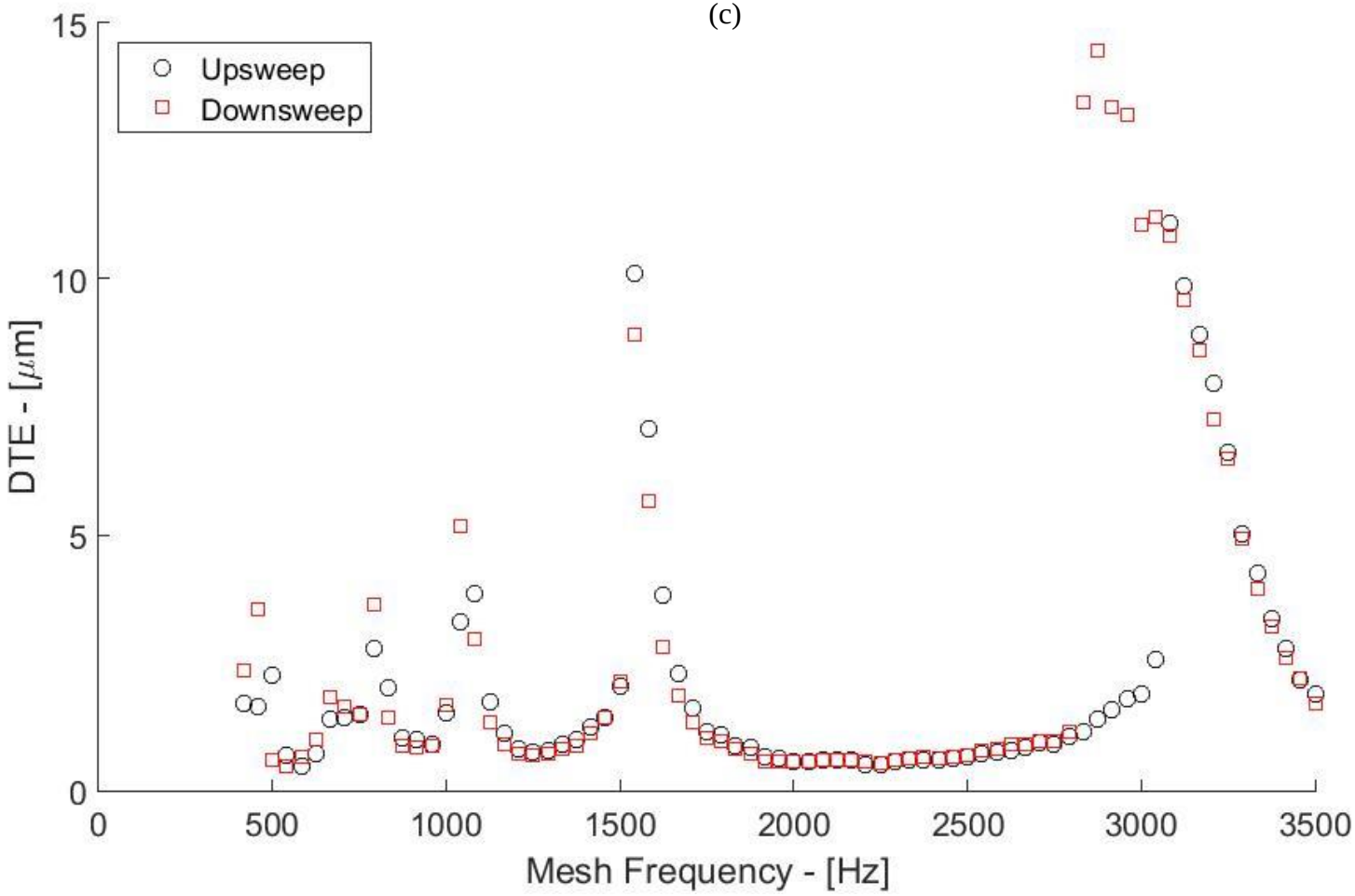

It is noted in Figure 3.2 that the measured RMS amplitudes of DTE are rather small. For instance, in Figure 3.2(c) at 300 Nm, the DTE amplitudes are typically less than 2 μm in the off-resonance ranges. The sweep-up and sweep-down values match remarkably well in these areas in spite of the very small vibration amplitudes seen. This clearly indicates the accuracy and sensitivity of the accelerometer-based DTE measurement system presented in Figure 2.6 and Figure 2.7.

3.2.2 Transient Measurements

The results from the transient (ramp-up, dwell and ramp-down) tests described in Chapter 2 are presented in this section. Figure 3.3(a-c) show these waterfall plots at transmitted torque values of 100, 200, and 300 Nm, respectively. These plots omit the first 50 Hz of frequency data since the DTE acceleration data was pseudo-integrated according to Eq. (2.5). The waterfall plots of Figure 3.3 clearly demonstrate the following:

(i) It is clear that there only one natural frequency within the speed range of operation, confirming that the gear pair behaves in a torsional manner.

(ii) The first three harmonic orders (increasing or decreasing diagonally along straight lines) are prominent at all torque values while 4^{th} and 5^{th} harmonic orders are also detectable in Figure 3.3(c) at 300 Nm.

(iii) The large DTE amplitudes resulting resonances are evident in the frequencies when the diagonal order lines intersect the constant natural frequency line.

(iv) An increase in the natural frequency with increasing torque is demonstrated.

(a)

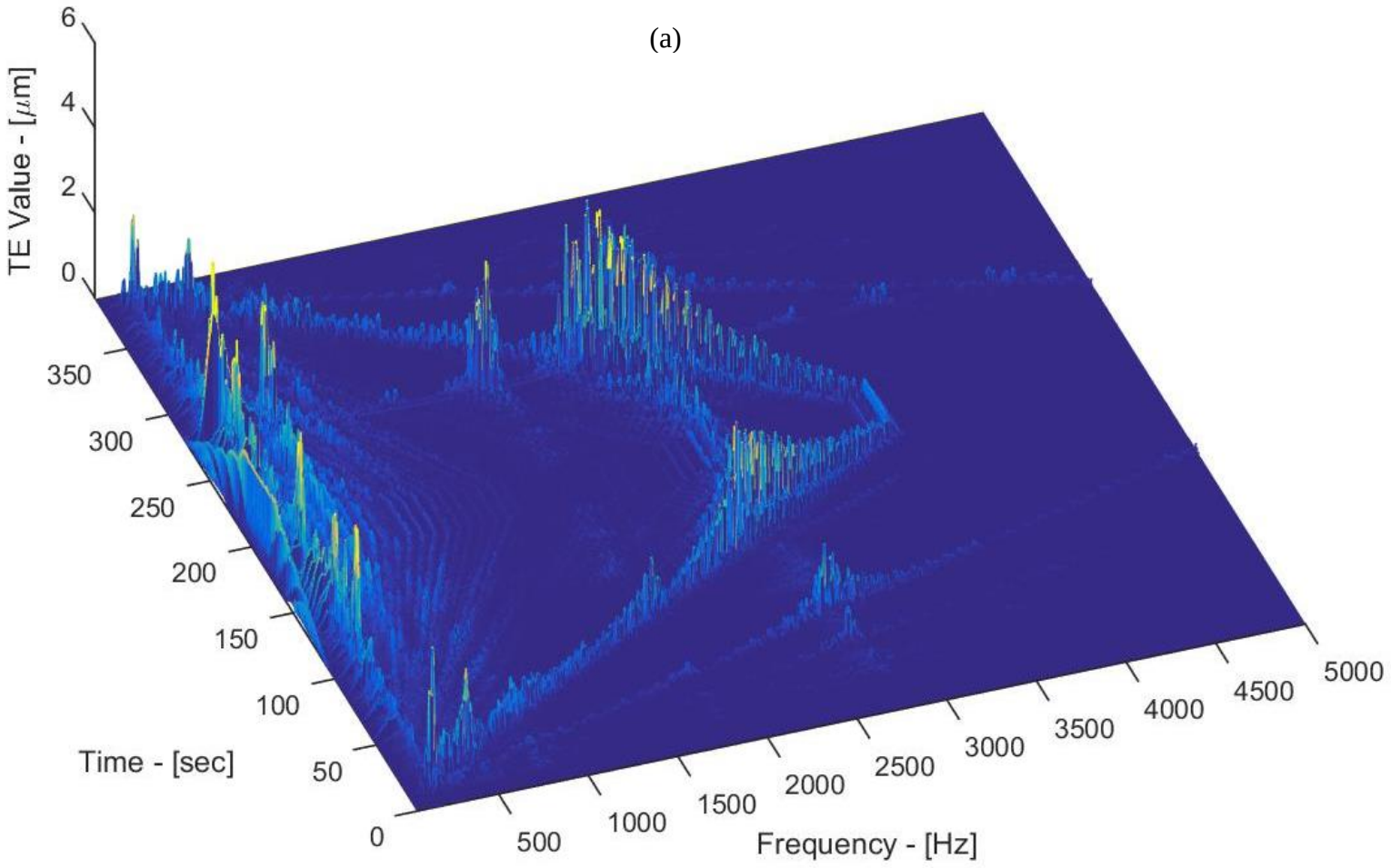

Figure 3.3: Full sweep up, dwell, and sweep down transient waterfall plot for (a) 100Nm, (b) 200Nm, and (c) 300Nm transmitted load.

Figure 3.3 continued.

(b)

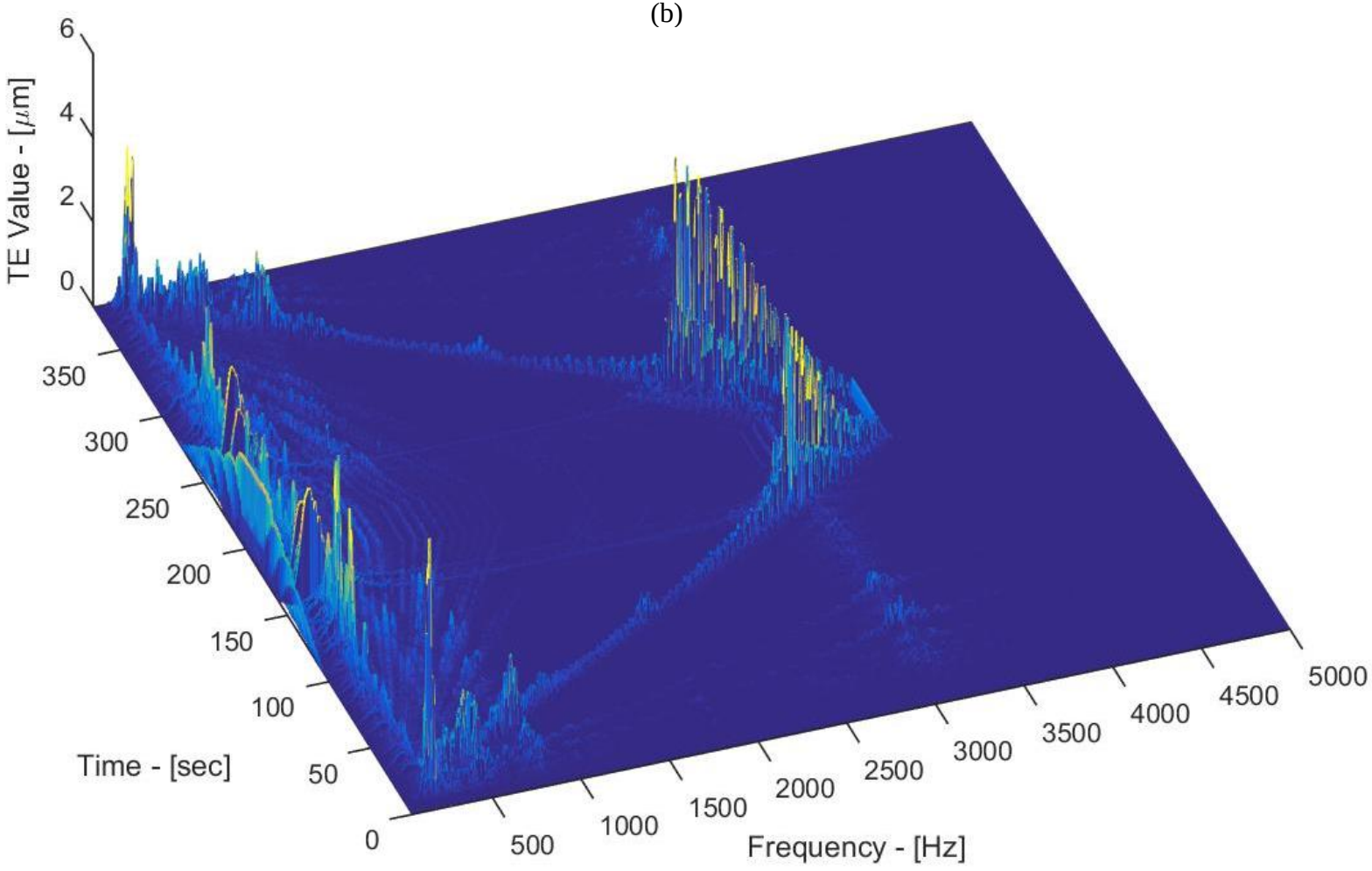

Figure 3.3 continued.

(c)

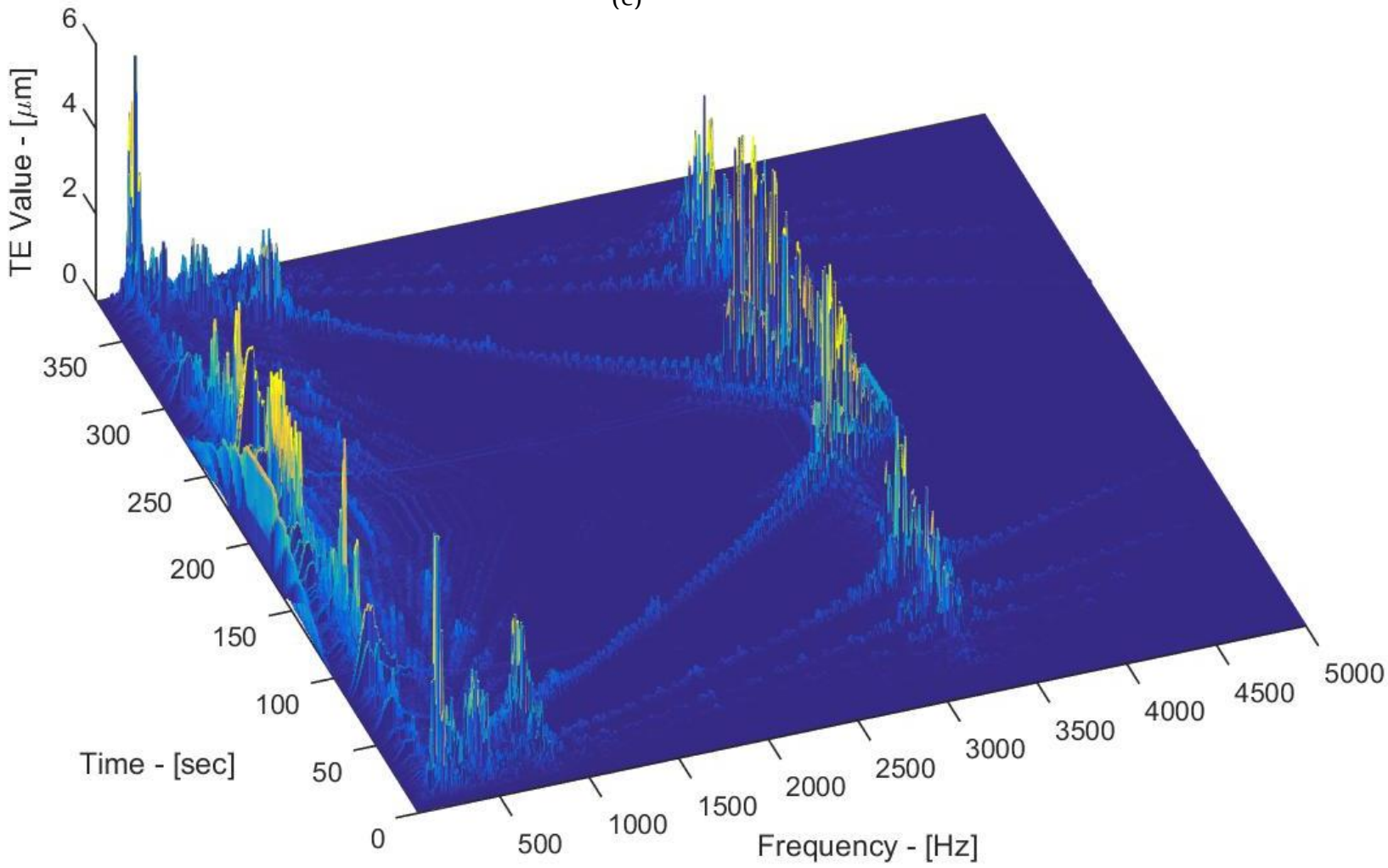

(v) The waterfall plots during the ramp-up and ramp-down portions of the waterfall plots exhibit sudden increases and sudden decreases in DTE, respectively, near the resonances due to nonlinear behavior exhibited. These "jump discontinuities" will be discussed later in detail. The same waterfall plots are separated to their ramp-down and ramp-up portions in Figure 3.4, Figure 3.5, and Figure 3.6, at 100, 200, and 300 Nm, respectively, to demonstrate the differences in amplitudes and frequencies of these jumps.

3.3 Nonlinear Dynamic Behavior

Gear pairs must be designed to have certain amount of clearance for various operational reasons such as accommodating center distance variations due to manufacturing errors and deflections, and providing a passage for lubricant to flow to reduce pocketing power losses. What keeps the gear teeth in contact – and ensures the designed clearance does not interfere with the gear pair – is the mean force transmitted. Yet, as described mathematically in Refs. [23, 24], under certain dynamic conditions defined by the fluctuations in mesh stiffness, damping, transmitted force, and operating speed, vibrational amplitudes might become large enough to overcome static deflections of the tooth pairs, and cause intermittent loss of contact during portions of mesh cycle. This nonlinear behavior was captured experimentally in Refs. [18-20, 23, 24] for spur gears, and was shown to not be evident in helical gears [21]. The spur gears tested in this study are not exceptions to these earlier observations.

(a)

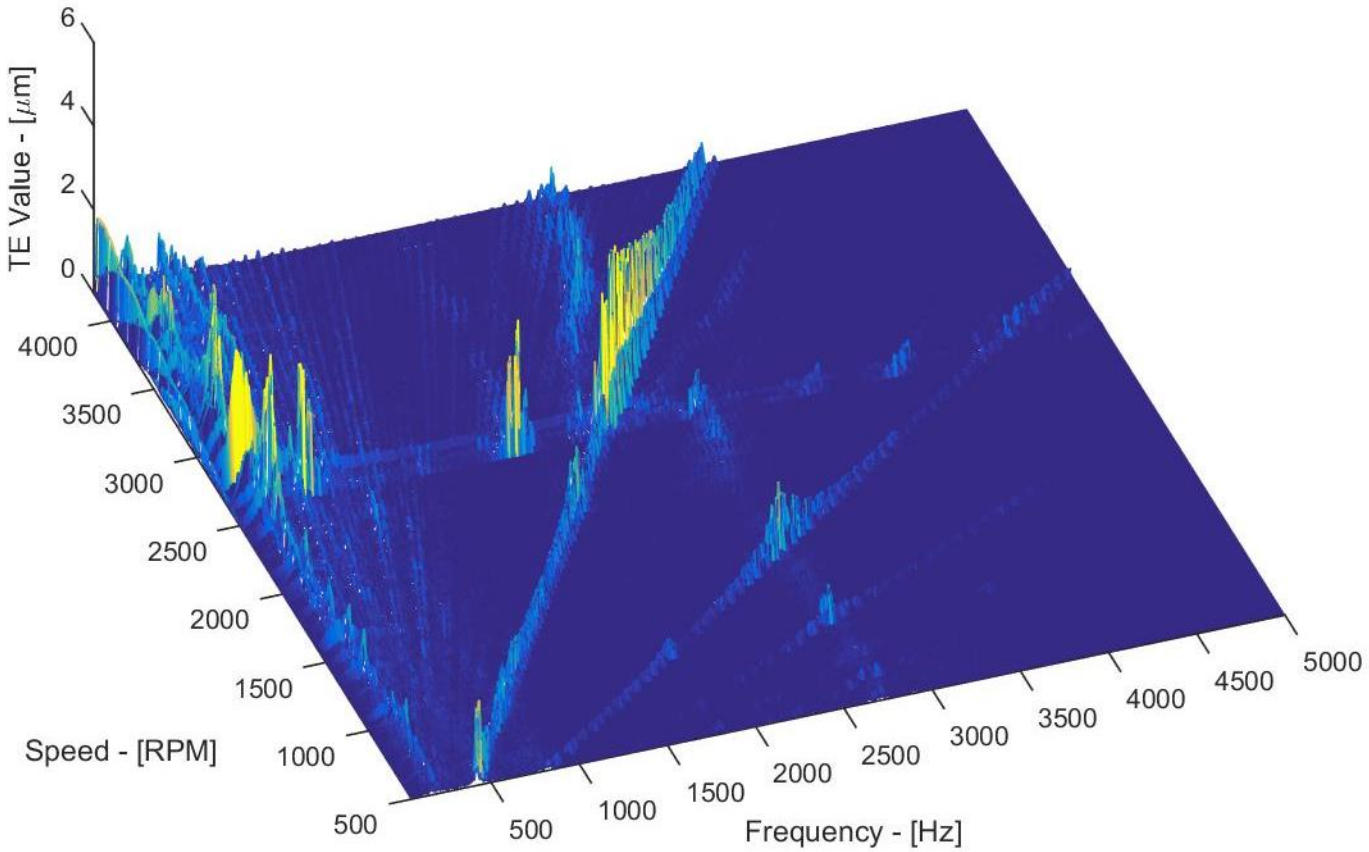

Figure 3.4: Waterfall plots of DTE during (a) ramp-down and (b) ramp-up conditions at 100 Nm.

Figure 3.4 continued.

(b)

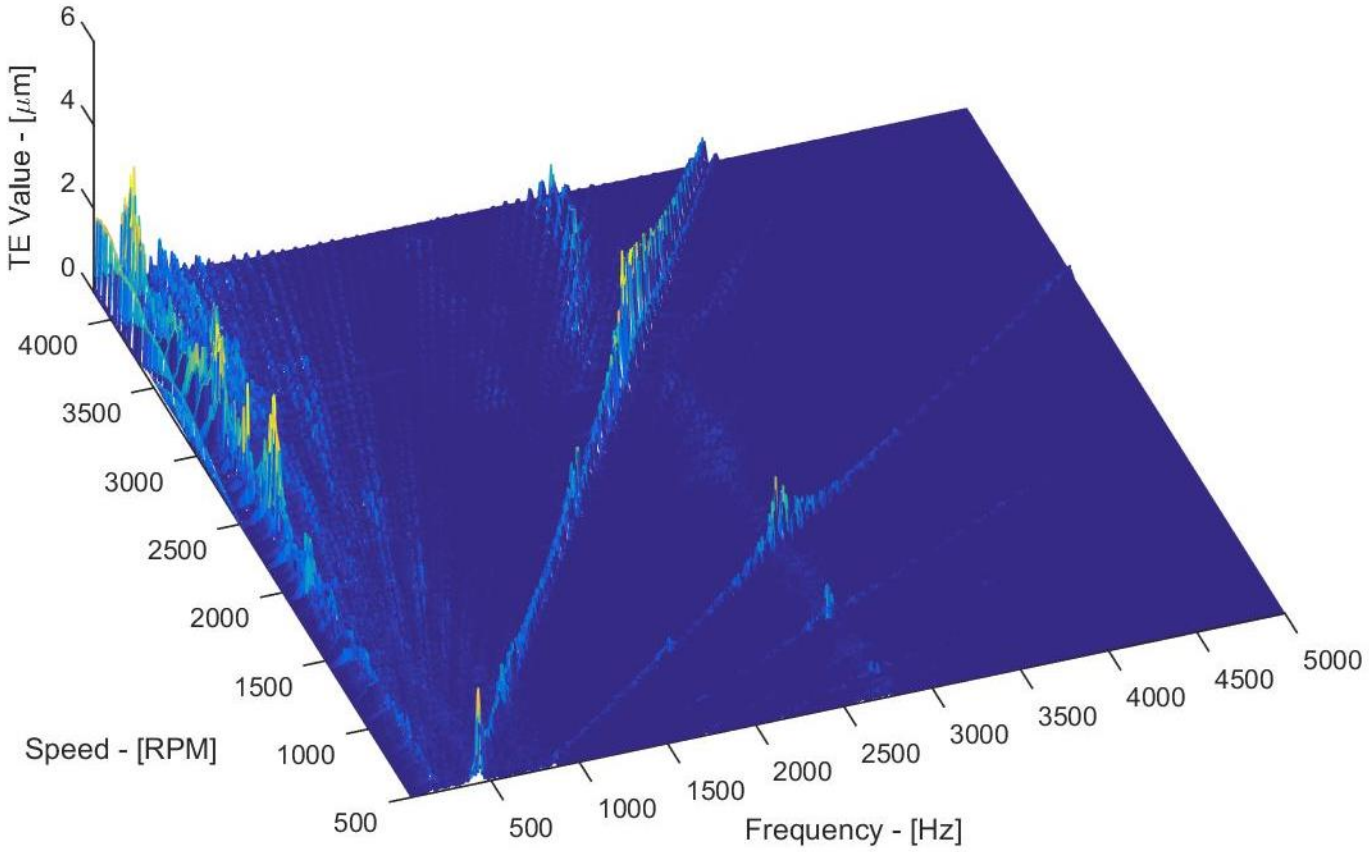

(a)

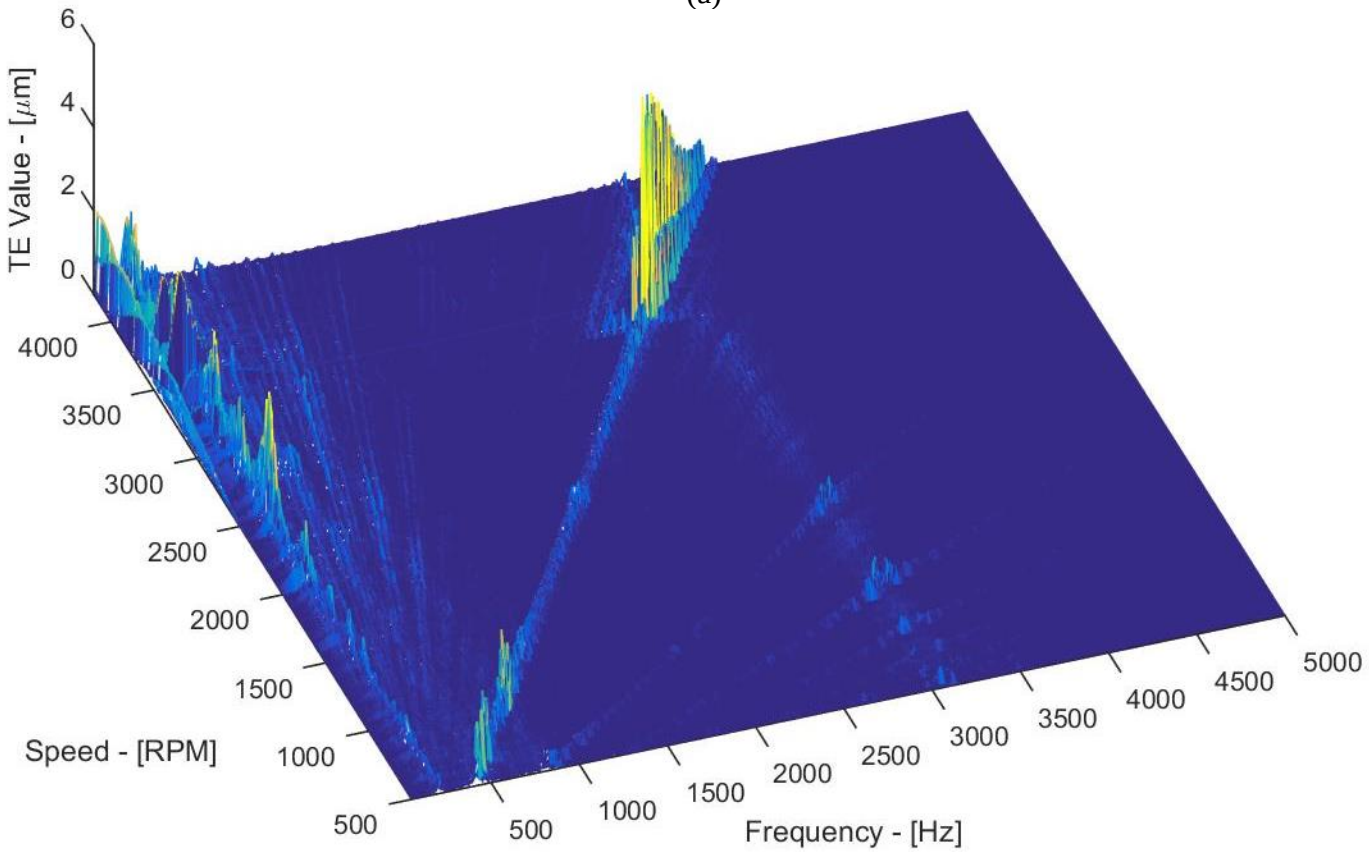

Figure 3.5: Waterfall plots of DTE during (a) ramp-down and (b) ramp-up conditions at 200 Nm.

Figure 3.5 continued.

(b)

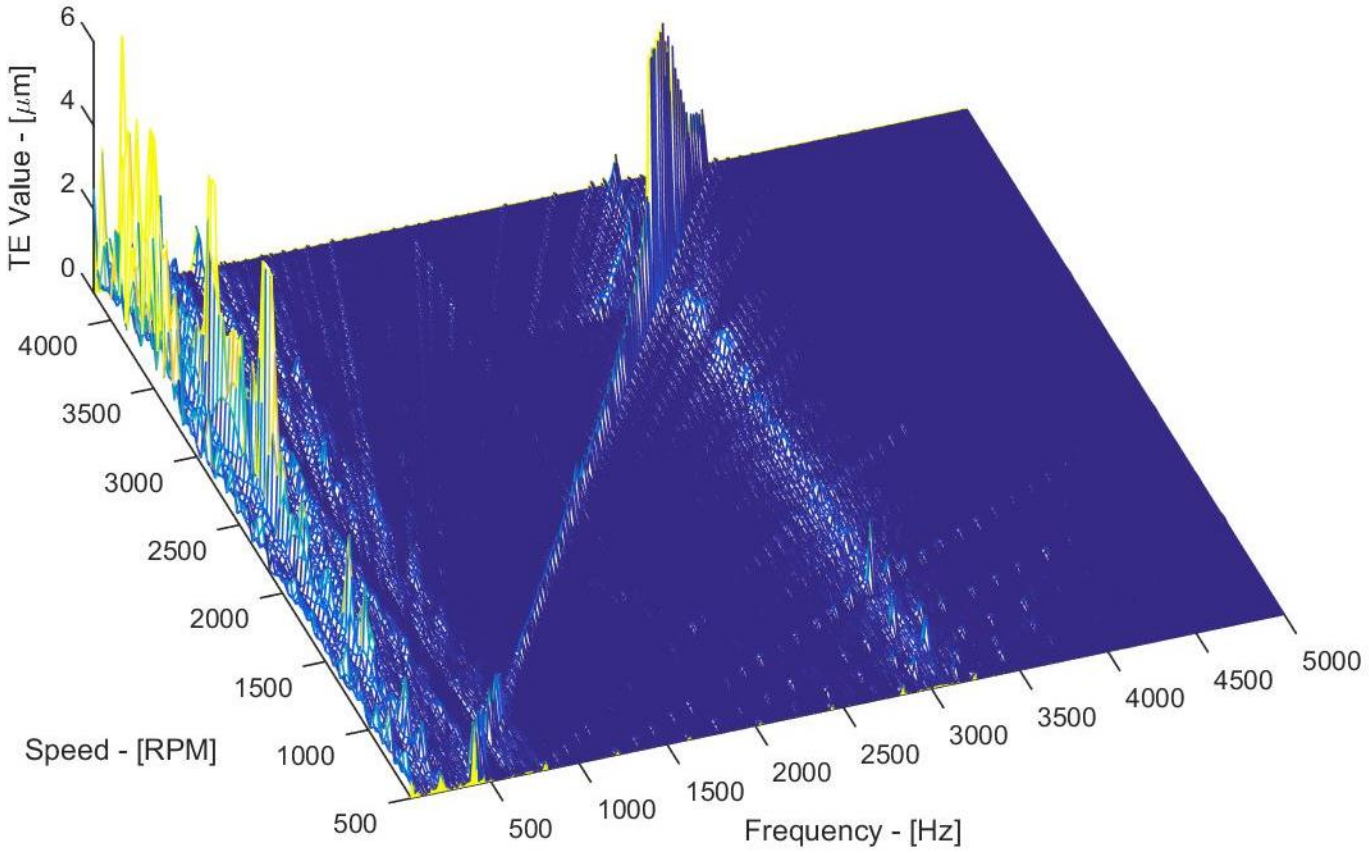

(a)

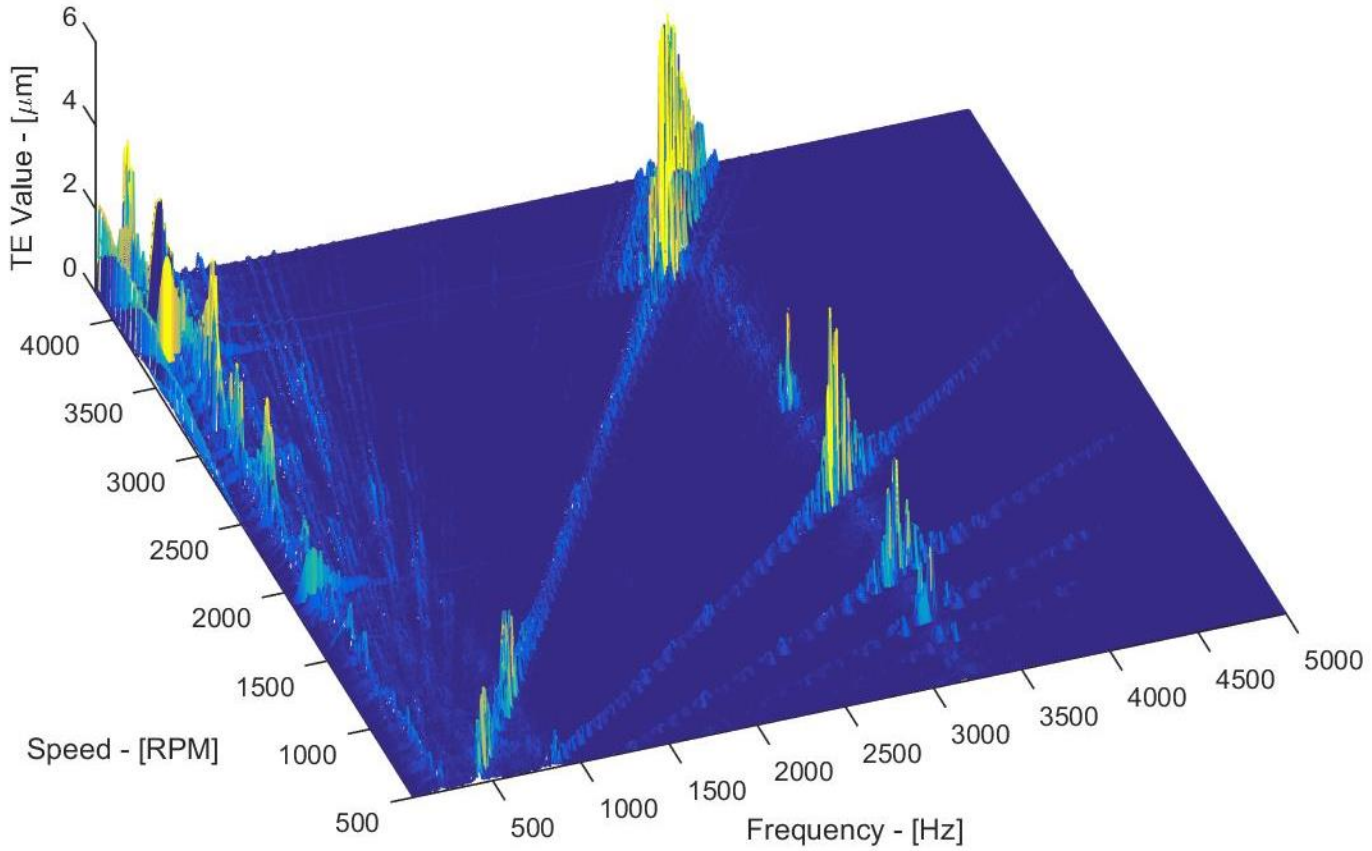

Figure 3.6: Waterfall plots of DTE during (a) ramp-down and (b) ramp-up conditions at 300 Nm.

Figure 3.6 continued.

(b)

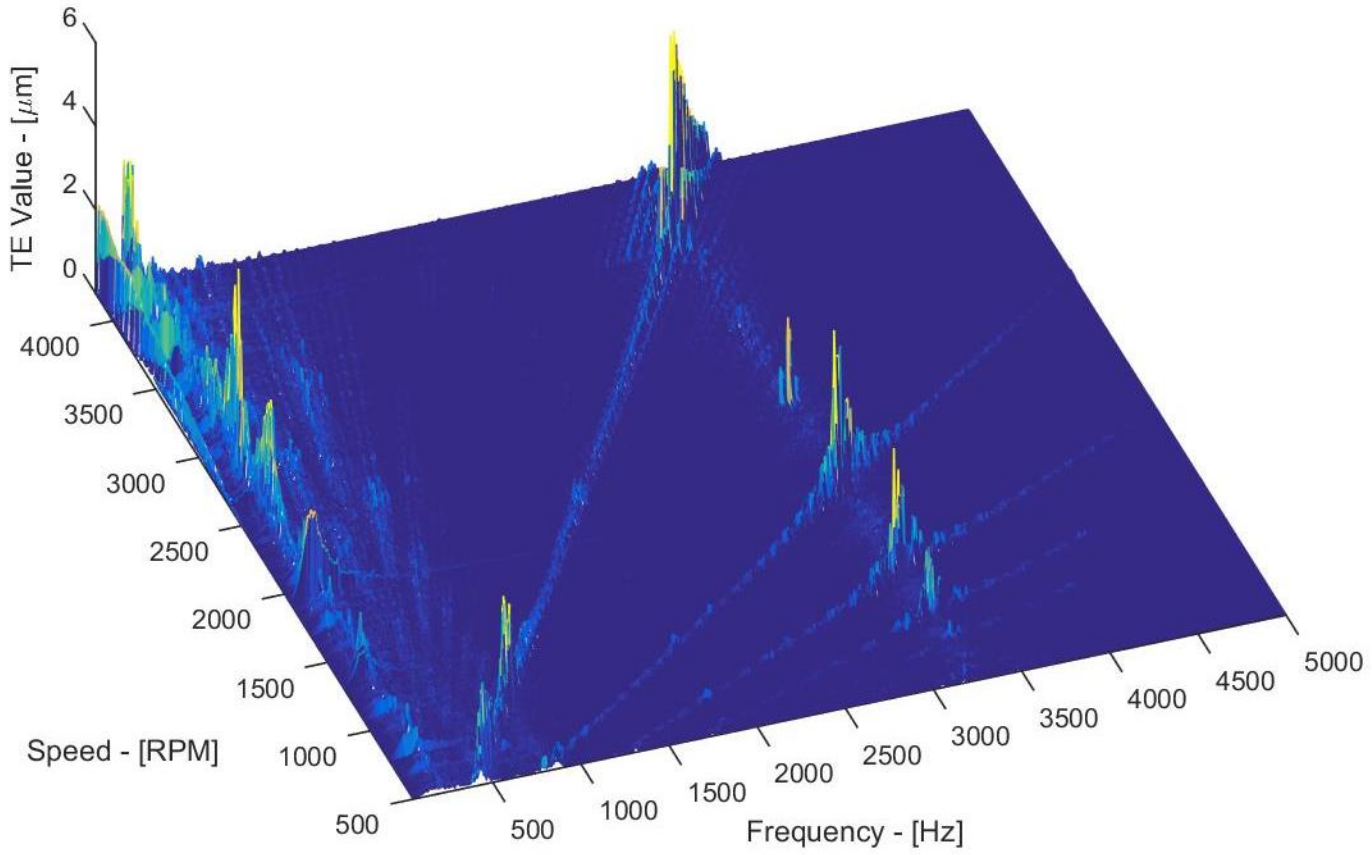

The most notable nonlinear behavior occurs around the fundamental resonant peak, and to a certain extent around the first super-harmonic resonance peak, as evident in the forced response curve of Figure 3.7 at 300 Nm. As the test progressed at increasing steady-state speed steps, the RMS value of the DTE amplitude at 3050 Hz suddenly increased from 2.5 μm to nearly 11 μm with only a slight increase in operating speed (and therefore mesh frequency). This sudden jump-up discontinuity in amplitude is marked by an upward pointing arrow on Figure 3.7. Further increases in operating speed beyond this jump-up frequency caused the DTE amplitudes to decay as the mesh frequency moved away from the resonance frequency.

Sweep-down tests starting at 3500 Hz followed the path established by the sweep-up tests all the way to the jump-up frequency. At this point, the response curve amplitude continued to increase, instead of following the down sweep data. At 2800 Hz, the DTE amplitude of 14 μm reduced suddenly to 1 μm with a slight reduction in speed, with this jump-down discontinuity depicted by a downward arrow in Figure 3.7.

Between the jump-down and jump-up frequencies of 2800 and 3050 Hz, two stable motions (along with an unstable one in between which cannot be shown experimentally) are present with two branches of motions. The lower branch motions are nearly linear and have low amplitudes. They can only be experimentally seen through sweep-up operation (i.e. by approaching from the lower frequencies). Meanwhile, higher branch motions (at higher amplitudes) exhibit significant tooth separation activity and can be only be experimentally seen through sweep down operation (i.e. by approaching from higher frequencies). While these separations might not be entirely obvious from all of the DTE

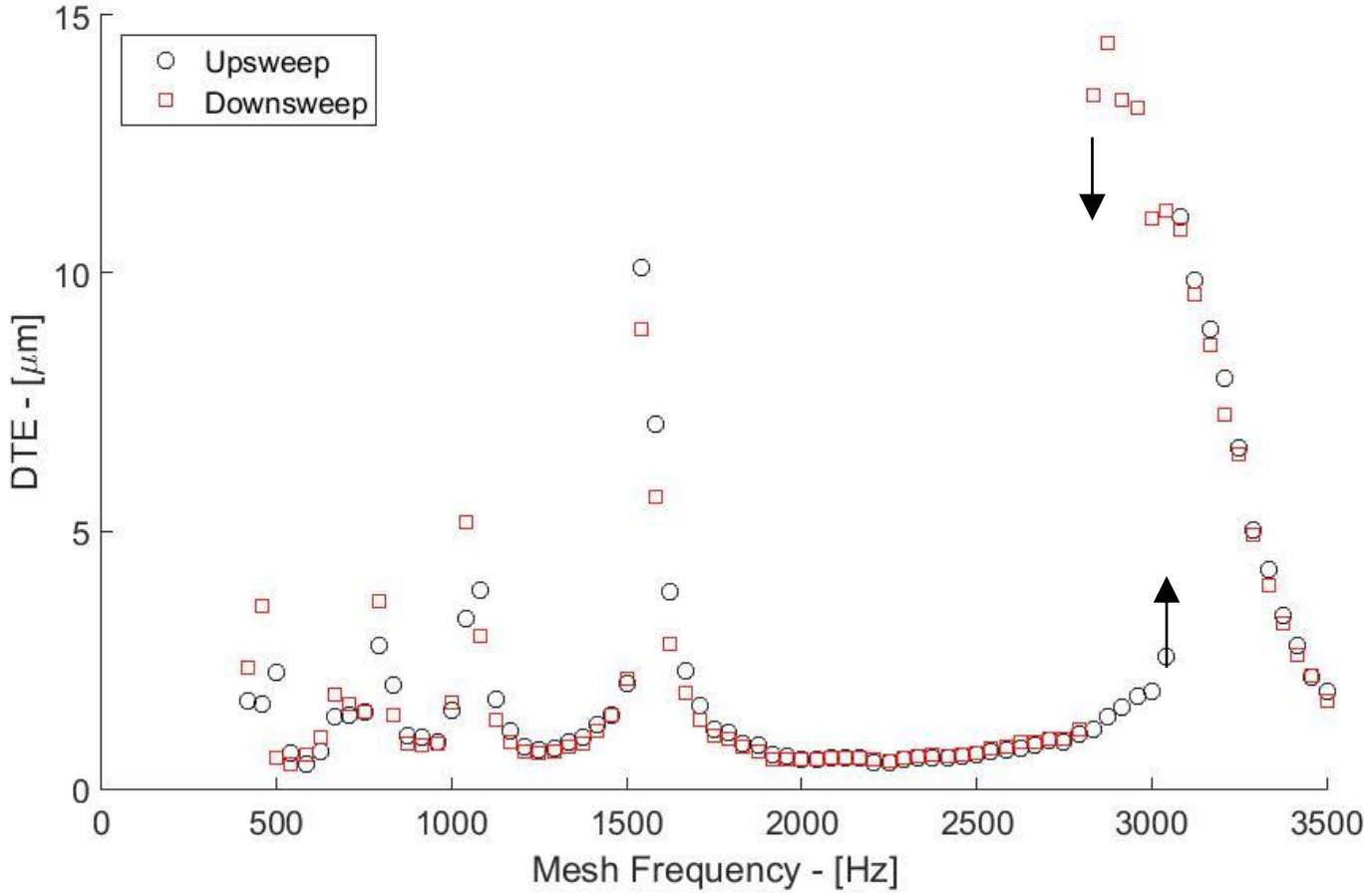

Figure 3.7: DTE RMS showing clear existence of jump discontinuities around the fundamental resonance peak at 300 Nm.

time histories herein, root stress time histories of Sun [25] and Hotait and Kahraman [28] clearly demonstrate them.

In Figure 3.8(a-b), time histories and the corresponding FFT spectra of lower and upper branch DTE at 2800 Hz (right before the jump-down takes place) are shown. Figure 3.8(a) exhibits the very low amplitude response of the gear pair on the lower branch, while Figure 3.8(b) exhibits the corresponding upper branch motion that is an order of magnitude larger that its lower branch counterpart. Both of these motions are dictated by the initial conditions of operation (where the motion starts). The same initial conditions map (initial velocity versus initial displacement) is divided into two domains, one attracting the upper branch motion and the other lower branch.

3.4 Influence of Torque Transmitted

In their experimental investigation of the influence of involute contact ratio on the resulting vibrations of spur gears, Kahraman and Blankenship [19] showed that the actual contact ratio (average number of tooth pairs in contact) increased with increasing torque. This increase subsequently increased the average gear mesh stiffness $\bar{k}_{mesh}$, causing an increase in the system natural frequency, f_n, in accordance with Eq. (3.1). As $\bar{k}_{mesh}$ is the square root in this equation, this relationship was shown to be slightly nonlinear. Figure 3.9 displays all the plots of Figure 3.2 in the same chart to show the influence of torque on

(a)

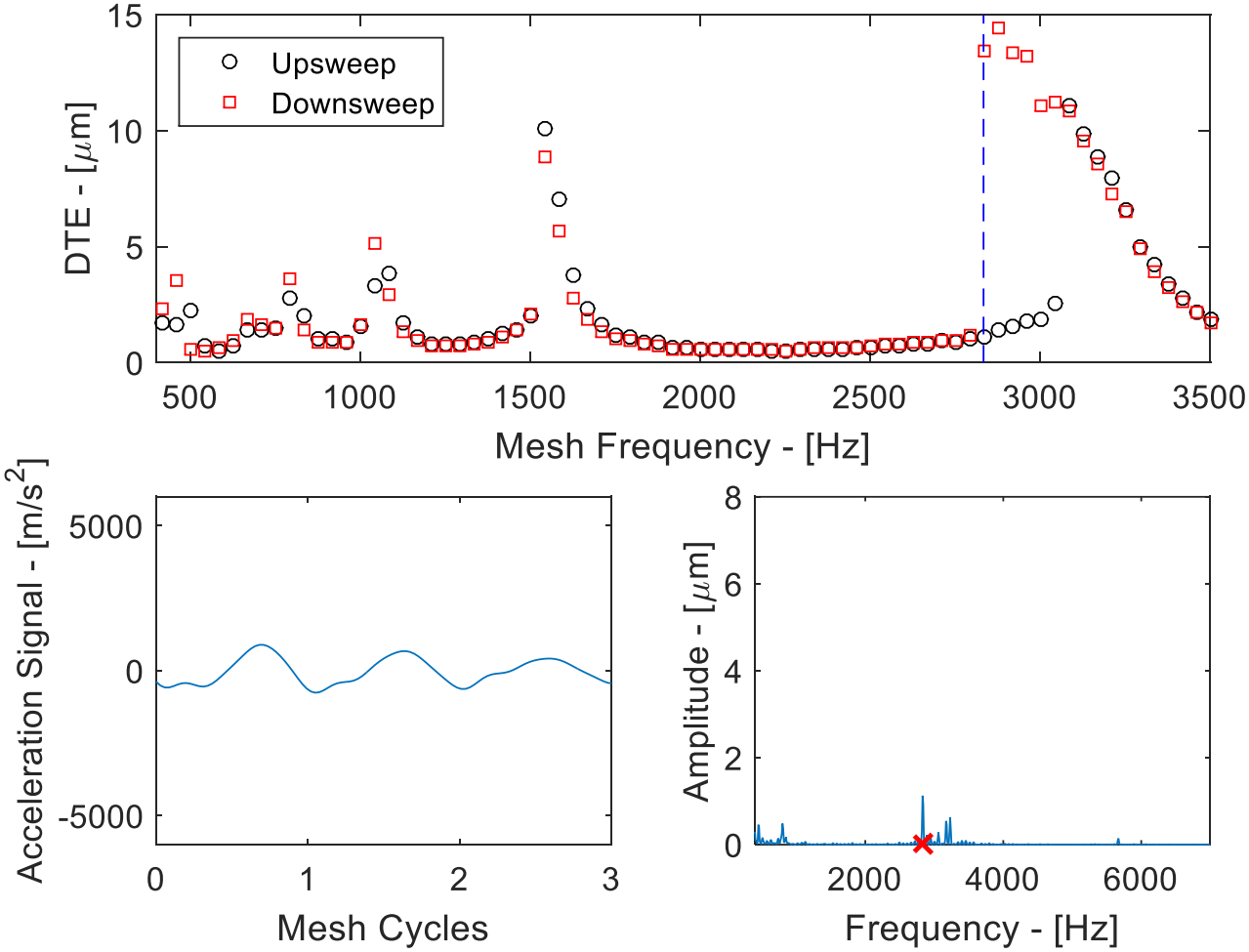

Figure 3.8: RMS DTE plot across the entire speed range (top), along with a 3-Mesh Cycle time domain plot (bottom left) and a FFT frequency domain plot (bottom right) for the 300Nm torque load (a) sweep up and (b) sweep down conditions.

Figure 3.8 continued.

(b)

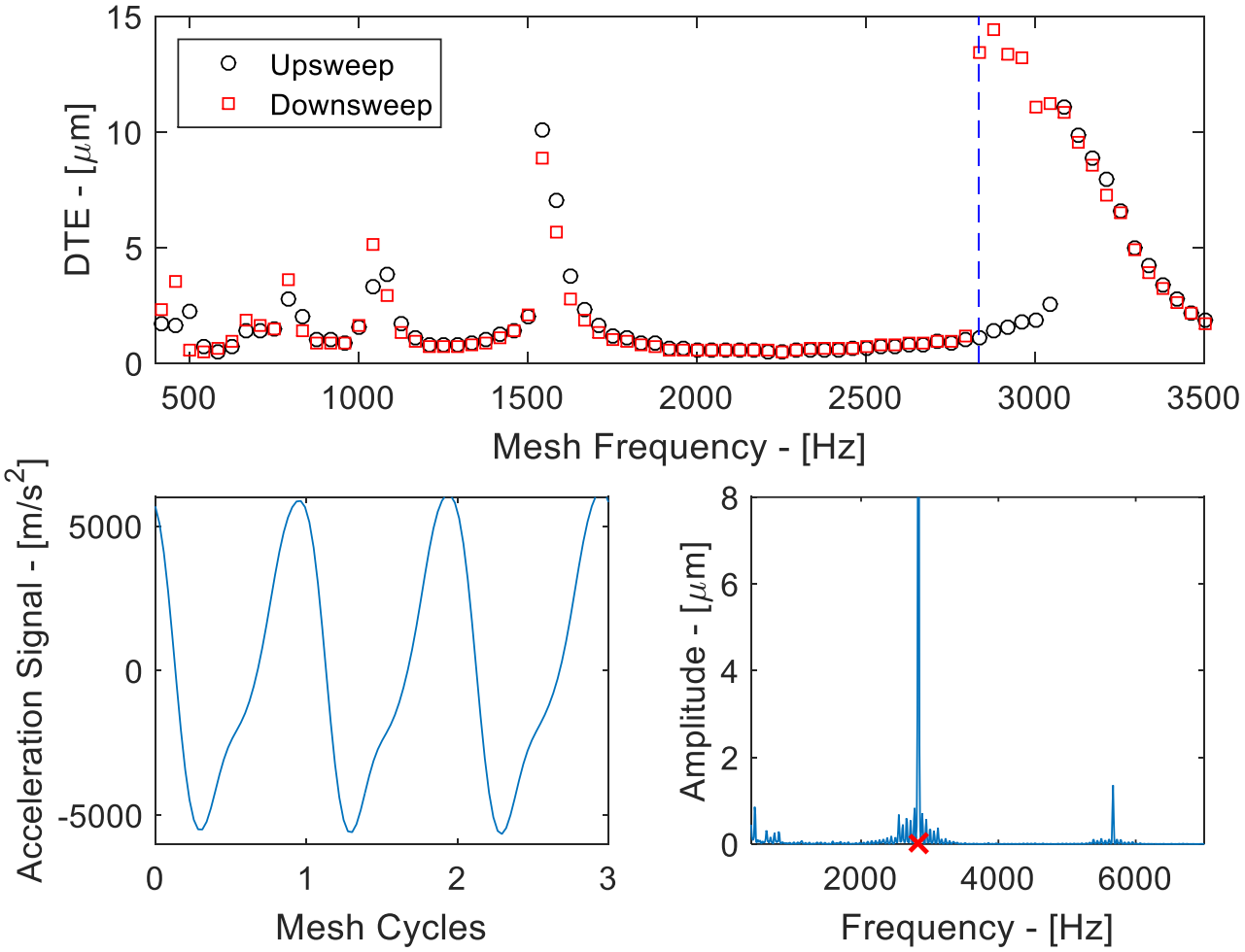

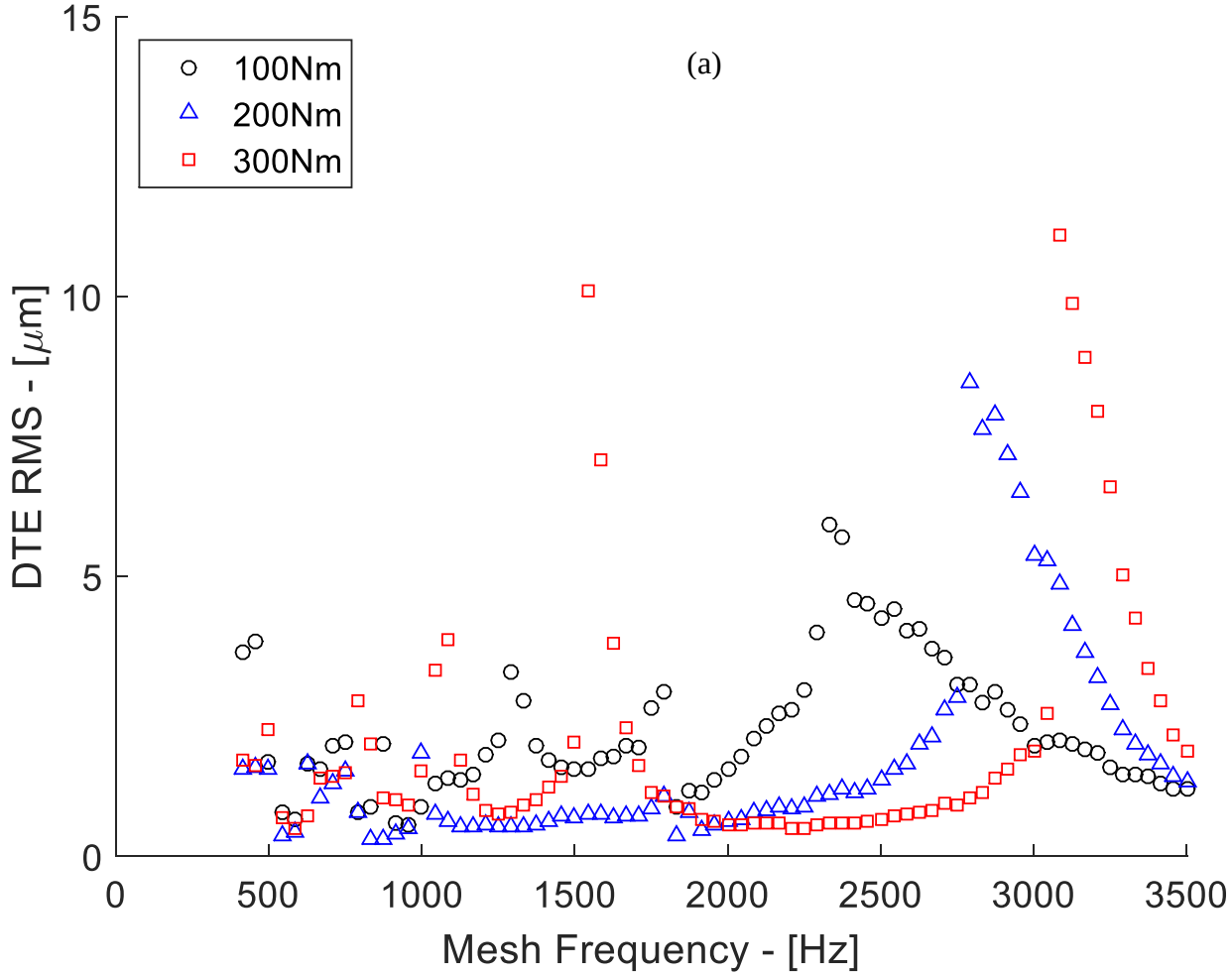

Figure 3.9: RMS DTE plot showing all three torque loads (100Nm, 200Nm, and 300Nm) and the changes in fundamental resonant frequency seen at each for the (a) sweep up and (b) sweep down conditions.

Figure 3.9 continued.

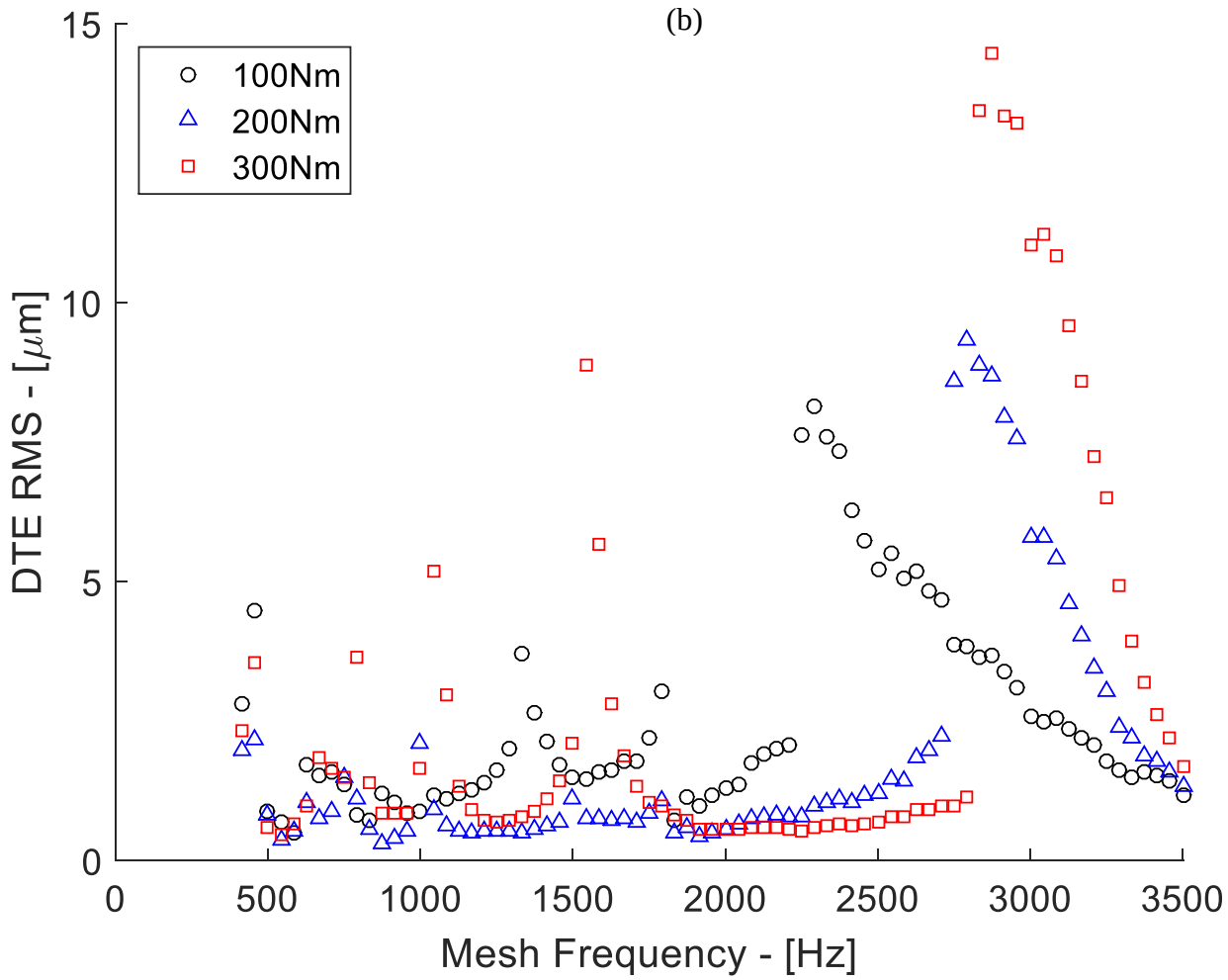

the forced response. With the help of waterfall plots of Figure 3.3, it can be determined that f_n = 2600, 3100, and 3300 Hz at 100, 200, and 300 Nm, respectively, which is in agreement with Figure 3.9. An increase of torque from 100 to 300 Nm causes a roughly 27% increase in f_n, which means $\bar{k}_{mesh}$ is increased nearly 52% in the process.

The other primary influence of torque transmitted on the spur gear pair relies heavily on the tooth modifications applied to the gear teeth. It was reported in Ref. [28] that these test gears, with the modifications specified in Table 2.1, were optimally operated at a transmitted torque of 300 Nm. In other words, the tooth modification magnitudes were comparable to the tooth deflection amplitudes seen at 300 Nm of transmitted torque, therefore reducing the amplitudes seen in the non-resonant regions at this particular loading condition. As such, the off-resonance DTE amplitudes at 300 Nm are lower than those at other torque levels, as shown in Figure 3.9.

Chapter 4:

Conclusion

4.1 Summary

This study was completed in order to develop an experimental characterization of a minimal-error spur gear pair. The primary focus of this work was on development of an accurate and reliable accelerometer-based dynamic transmission error measurement system. Upon completion of this measurement system – which included efficient, purpose-built data analysis systems – a family of baseline tests were completed across a broad ranges of operating speed, torque, and in both sweep up and sweep down configurations, in order to characterize the minimal-error gear pair as a means of baseline comparison for use within future studies.

4.2 Major Conclusions

Based on the results as discussed previously, the following general characterizations of the minimal-error spur gear pair can be made:

(i) At the 300Nm design load, the gear pair exhibited significant excitations at the system's fundamental resonant frequency of 3250 Hz.

(ii) Super-harmonic resonances existed across the operating range, and can clearly be captured by the dynamic test machine up to the fifth harmonic for most operating conditions.

(iii) Transient and steady-state measurements were shown to complement each other in terms of natural frequency and jump discontinuities.

(iv) The gear pair exhibited significant softening type jump nonlinearities about the fundamental resonant frequency depending on sweep up or sweep down operation, as described in Kahraman and Singh's work [17]. This nonlinearity existed at lower order super-harmonic resonances as well, albeit at a smaller magnitude.

(v) As torque load was decreased, so was the accompanying system fundamental resonant frequency, shifting to 3100 Hz and 2600 Hz at 200Nm and 100Nm torque load, respectively.

4.3 Future Work

The completion of this study provides a significant first step towards a MS thesis, which will utilize the results herein as a baseline condition upon which experimental comparisons can be made. The accompanying study will focus on a significant gap in current literature surrounding the vibrational dynamic behavior (and associated DTE) resulting from spur gear tooth indexing errors. The resulting study will act as a natural extension to Sun [25], with work intending to:

(i) Develop an accurate and reliable axial and rocking motion vibratory measurement system, in addition to the dynamic transmission error system herein, similar to the system introduced by Kang and Kahraman [8].

(ii) Develop a suitable explanation of the dynamic vibratory behavior seen as a result of tightly controlled manufactured tooth indexing errors on parallel axis spur gears.

(iii) Investigate the relationship between the root stresses (as previously studied [25]) and dynamic transmission error caused due to tooth indexing errors.

References

[1] Welbourn, D.B., “Fundamental Knowledge of Gear Noise - a Survey”, The Institution of Mechanical Engineers, London, **177** (1979), 9-14.

[2] Harris, S.L., “Dynamic Loads on the Teeth of Spur Gears, Proceedings of the Institution of Mechanical Engineers, **172** (1958) 87-112.

[3] Tordion, G.V. and Gerardin, H., “Dynamic Measurement of Transmission Error in Gears”, JSME Semi-Int. Symp., Sept., pp. 279-284, 1967.

[4] Munro, R.G., “A Review of the Theory and Measurement of Gear Transmission Error”, Int. Conference on Gear Noise and Vibration, Institute of Mechanical Engineers, pp. 2, 1990.

[5] Smith, J.D., *Gear Noise and Vibration,* New York: CRC Press, 1999.

[6] Houser, D.R. and Blankenship, G.W., “Methods for Measuring Gear Transmission Error Under Load and at Operating Speeds”, SAE Technical Paper Series, 1989.

[7] Heskamp, M., “Development of a Digital Data Acquisition and Analysis System for the Measurement of Dynamic Transmission Error of Spur and Helical Gear Pairs”, Master’s Thesis, The Ohio State University, 2009.

[8] Kang, M. and Kahraman, A., “Measurement of Vibratory Motions of Gears Supported by Compliant Shafts,” Mechanical Systems and Signal Processing, **29** (2012), 391-403.

[9] Gregory, R.W., Harris, S.L., and Munro, R.G., "Torsional Motions of a Pair of Spur Gears", Proceedings of the Institution of Mechanical Engineers, **178** (1963), 166-173.

[10] Gregory, R.W., Harris, S.L., and Munro, R.G., "Dynamic Behaviour of Spur Gears", Proceedings of the Institution of Mechanical Engineers, **178** (1963), 207-218.

[11] Tuplin, W.A., "Dynamic Loads on Gear Teeth", Machine Design, pp 203, Oct. 1953.

[12] Cornell, R.W. and Westervelt, J., "Dynamic Tooth Loading for High Contact Spur Gears", Journal of Mechanical Design, **100** (1978), 69-76.

[13] Velex, P., "On the Modelling of Spur and Helical Gear Dynamic Behaviour", Mechanical Engineering, ISBN: 978-953-51-0505-3, pp 75-106, 2012.

[14] Lin H.H. and Liou C.H., "A Parametric Study of Spur Gear Dynamics", NASA/CR-1998-206598.

[15] Seireg, A. and Houser, D.R., "Evaluation of Dynamic Factors for Spur and Helical Gears", Journal of Engineering for Industry, **92** (1970), 504-514.

[16] Ozguven, H.N. and Houser, D.R., "Mathematical Models Used in Gear Dynamics—A Review", Journal of Sound and Vibration, **121** (1988), 383-411.

[17] Kahraman, A. and Singh, R., "Non-Linear Dynamics of a Spur Gear Pair", Journal of Sound and Vibration, **142** (1990), 49-75.

[18] Kahraman, A. and Blankenship, G.W., "Experiments on Nonlinear Dynamic Behavior of an Oscillator with Clearance and Periodically Time-Varying Parameters", Journal of Applied Mechanics, **64** (1997), 217-226.

[19] Kahraman, A. and Blankenship, G.W., "Effect of Involute Contact Ratio on Spur Gear Dynamics", Journal of Mechanical Design, **121** (1999), 112-118.

[20] Kahraman, A. and Blankenship, G.W., "Effect of Involute Tip Relief on Dynamic Response of Spur Gear Pairs", Journal of Mechanical Design, **121** (1999), 313-315.

[21] Kubur, M., Kahraman, A., Zini, D., and Kienzle, K., "Dynamic Analysis of a Multi-Shaft Helical Gear Transmission by Finite Elements: Model and Experiment," Journal of Vibrations and Acoustics, **126** (2004), 398-406.

[22] Litak, G. and Friswell, M.I., "Nonlinear Vibration in Gear Systems", Nonlinear Dynamics of Production Systems, ISBN: 978-352-76-0258-2, pp 339-348, 2005.

[23] Blankenship, G. W. and Kahraman, A., "Steady State Forced Response of a Mechanical Oscillator with Combined Parametric Excitation and Clearance Type Nonlinearity," Journal of Sound and Vibration, **185** (1995), 743-765.

[24] Kahraman, A. and Blankenship, G. W., "Interaction between External and Parametric Excitations in Systems with Clearance," Journal of Sound and Vibration, **194** (1996), 317-336.

[25] Sun, A. "An Experimental Study of the Dynamic Response of Spur Gears Having Tooth Index Errors", M.S. Thesis, The Ohio State University, Columbus, OH, 2015.

[26] Munro, R.G., Yildirim N., and Hall, D.M., "Optimum Profile Relief and Transmission Error in Spur Gears," IMechE Conference on Gearbox Noise and Vibration, 1990, Paper C404/032, pp 35–41.

[27] Palmer, D., "The Effects of Profile Relief on Narrow Face Width Parallel Axis Gears," Ph.D. Dissertation, Huddersfield University, 1999.

[28] Hotait, M.A., and Kahraman, A., “Experiments on the relationship between the dynamic transmission error and the dynamic stress factor of spur gear pairs”, Mechanism and Machine Theory, **70** (2013), 116-128.